Negative rectification and anomalous diffusion in nonlinear substrate potentials: Dynamical relaxation and information entropy

Yuhui Luo,[1,2] Chunhua Zeng,[1,*] and Baowen Li[3]

[1]*Faculty of Civil Engineering and Mechanics/Faculty of Science, Kunming University of Science and Technology, Kunming 650500, China*

[2]*School of Physics and Information Engineering, Zhaotong University, Zhaotong 657000, China*

[3]*Paul M. Rady Department of Mechanical Engineering and Department of Physics, University of Colorado, Boulder, Colorado 80309-0427, USA*

(Received 18 October 2021; accepted 12 January 2022; published 23 February 2022)

We numerically investigate the rectification of the probability flux and dynamical relaxation of particles moving in a system with and without noise. The system, driven by two external forces, consists of two substrate potentials that have identical shapes and different potential barriers with different friction coefficients. The deterministic model exhibits the perfect rectification of the probability flux, ratchet effect, and the dependence of the unpredictability of the dynamics on basin of attraction. In contrast, the stochastic model displays that the rectification is sensitive to the temperature and an external bias. They can induce kinetic phase transitions between no transport and a finite net transport. These transitions lead to an unexpected phenomenon, called negative rectification. The results are analyzed through the corresponding time-dependent diffusion coefficient, information entropy (IE), etc. At a low temperature, anomalous diffusions occur in system. For the occurrence of the flux in certain parameter regimes, the larger the diffusion is, the smaller the corresponding IE is, and vice versa. We also present the selected parameter regimes for the emergence of the rectification and negative rectification. Additionally, we study the rectification of the interacting particles in the system and find that the flux may depend on the coupling strength and the number of the interacting particles, and that collective motions occur for the forward flux. Our work provides not only a way of the rectification for the transport of various particles (e.g., ions, electrons, photons, phonons, molecules, DNA chains, nanoswimmers, dust particles, etc.) in physics, chemistry, biology, and material science, but also a design of various circuits.

DOI: 10.1103/PhysRevE.105.024204

I. INTRODUCTION

Rectification is ubiquitous in physical, chemical, and biological systems with asymmetry. Its application ranges from electron or quanta [1] to motile bacteria [2] or molecular junctions [3,4], even dust particles [5]. Namely, it ranges from the nanoscale to mesoscale. Thus, understanding and controlling the rectification of particles (e.g., ions, electrons, photons, phonons, molecules, DNA chains, nanoswimmers, dust particles, etc.) is an outstanding challenge for physics, chemistry, and biology, with relevance throughout materials science. A symmetrical system usually exhibits reciprocity of the flux. However, the reciprocity must be broken in an asymmetrical system that provides a one-direction flux of the particles, namely, the occurrence of rectification. There are many prominent examples of the rectifications for various particles in asymmetrical systems, i.e., the rectifications of the electrons, phonons [6,7], ions [8,9], molecules [10], light [11,12], heat of molecular junctions [3,4], spin chains [13], electronic heat flux [14], entropy production [15–17], nanoswimmers [18,19], dust particles [5], etc. Moreover, the most intriguing example is that Feynman ratchet, a device that rotates in only one direction, is able to rectify the thermal Brownian motion of gases held at two different temperatures [20]. Furthermore, typical examples for biology are the existence of the rectification of the anoctamin 1 current in nociceptive neurons [21], of the ion current in electronic skin [22], and of the elevated temperature-evoked current in TRPV-3-expressing cells [23]. These rectifications result in the invention for diodes of the electron, heat [6,7], quantum spin chains [13], superconductors [24], etc.

Besides the nonreciprocity-like transport of these particles, the nonreciprocity of the wave propagations is of great importance in science and technology as well [25–28], such as electromagnetic, acoustic, and mechanical wave propagation. These nonreciprocities provide the way for conversion and harvesting, soft robotics, sensor technologies, energy harvesting systems, acoustic imaging [25,26], the control of phonon modes [27], etc. Based on the above, a nonreciprocity or asymmetry is key to the occurrence of rectification. To understand the underlying mechanism of the rectification, other corresponding properties in these asymmetrical systems are of significant importance and particular interest, such as entropy and diffusion.

Since Einstein published his theory of Brownian motion in 1905 [29], the diffusion of Brownian particles has been of great importance in physics, chemistry, and biology, and has been in the research spotlight for more than 100 years [30–34]. Thus substantial progress has been made in the understanding

*zchh2009@126.com

of the underlying mechanism for the diffusion of Brownian motion [30–32]. However, the diffusion of various particles in liquid, including hydrodynamics and thermodynamics, remains a huge challenge since the friction is very complex. In particular, a Brownian particle moving in water experiences Stokes memoryless friction including the viscosity, while the particle moving in polymeric fluid experiences a friction with memory (corresponding to a fractional Langevin equation) [35]. Furthermore, a multiple-relaxation-time lattice Boltzmann kinetic model reveals that the viscosity takes part in both the thermodynamic and hydrodynamic responses [36]. It also indicates that boundary length and thermodynamics lead to the coupled Rayleigh-Taylor-Kelvin-Helmholtz instability system [37]. Therefore, the diffusion is still an open challenging question. Besides the development of the diffusive theory, its application is ubiquitous, such as in nematic liquid crystals [33]. Another typical example is lithium diffusion in Li-ion batteries [38,39] or LiPON electrolytes [40], which exhibits that the larger the diffusion coefficient is, the charge is faster. Moreover, anisotropic diffusion at boundaries can tune noise rectification and particle sorting [41].

Besides diffusion, another important quantity characterizing whether system is in disorder or not is information entropy (IE) [42,43]. It is also an order parameter to explore whether there exists a phase transition or not in a system. In general, most works employ diffusion to study the spreading of the position of the particle, and probability distribution of velocity to investigate the mobility of the particle. The Gaussian probability distribution corresponds to normal diffusion in certain models [33,44]. However, an arbitrary model for normal diffusion does not correspond to the Gaussian distribution of the velocity. Through the probability distribution of the velocity, we can obtain the IE of a system. Its drastic changes, resulting from a trivial variation of a system parameter, imply that a phase transition may arise in the system. Besides, other order parameters also present the evidence of a phase transition, i.e., a kinetic phase transition of the transport [45–47]. It is well known that the phase transition plays a crucial role in physics and material science.

To achieve rectification, we frequently study the physical mechanism of the transports (e.g., flux) of these particles. It is worth mentioning that there are a few works that have studied the noise-induced rectification in various systems with particular conditions, such as out-of-equilibrium structures [48], interacting Brownian ratchets [49], and noninteracting Brownian particles in two-dimensional artificial channels [50]. Notice that noise plays a key role, and its induced phenomena (i.e., resonant activation and noise enhanced stability) have been studied in various systems [51,52]. However, no works have been found to investigate the influence of the driving forces and thermal noise inducing the Brownian particle moving in an asymmetric system far away from equilibrium on rectification. The system consists of two different substrate potentials with the identical shapes of substrate potential and different potential barriers with different friction coefficients.

Notice that the transport of the particle is frequently manipulated through a system consisting of different materials. For example, the transport of the electron generally exhibits a current rectification in *p-n* junction. Additionally, the transport of the phonon shows the rectification of thermal flux at different substrate potentials [6]. In fact, these rectifications are positive. However, several systems, consisting of multiple complex materials, display the occurrence of negative rectifications, such as the negative rectifications in the armchair graphene nanoribbon *p-n* junctions with $3n+1$ width [53], nanopipettes [54], poly-L-lysine-coated quartz nanopipettes [55], nanoscale single-walled carbon nanotube *p-n* junctions [56], and dual-mode solid-state thermal rectification [57]. In short, a system with different potentials leads to its symmetry breaking, thus it becomes an asymmetrical system that can lead to certain rectification.

Based on the mentioned above, a natural question is whether negative rectifications are expected to hold for Brownian particles moving in an out-of-equilibrium system consisting of two different substrate potentials. If the answers are positive, what is the underlying physical mechanism behind the rectification? And what are the corresponding diffusion and IE for negative rectifications? To address these questions, we here focus on the rectification of the probability flux and the corresponding diffusions and IE of the particle moving in the system. It is driven by an external constant bias and an external time-dependent periodic force for the deterministic case and the presence of thermal noise. Furthermore, a significant and challenging task here is to systematically provide the bridging among flux rectification, diffusion, and IE. This will introduce more insight into the concept of rectification resulting from asymmetry and fill the existing gaps in understanding rectification and the corresponding diffusion and IE in particular.

The rest of the paper is organized as follows. We first present the basic model and method in Sec. II. There we present the flux of the particle for deterministic dynamics and analyze the findings through the basin of attraction, the phase-space map, etc. In Sec. III we consider a single Brownian particle moving in the system in the presence of thermal noise and present our results. These findings are analyzed through diffusion and IE. We also present the parameter regime in which the rectification arises. Next, we present the model and results of interacting Brownian particles in the presence of thermal noise. We discuss the applications of these findings and present our conclusions at the end.

II. THE DETERMINISTIC DYNAMICS

We consider an inertial particle with mass m moving in a system which consists of two different substrate potentials. They have the identical forms and different potential barriers. Namely, the system is given by [6]

$$U(q)=\begin{cases}U_l\sin(2\pi q) & q<0\\ U_r\sin(2\pi q) & q\geqslant 0\end{cases},$$

where U_l and U_r denote the potential barriers of the left and right substrate potentials, respectively. We employ $U_r=\lambda U_l$, where λ is the control parameter. Therefore, the potential in which the particle moves is described by the Hamiltonian [58–60]

$$H=\frac{p^2}{2m}+U(q)+\mathfrak{F}(t)q, \tag{1}$$

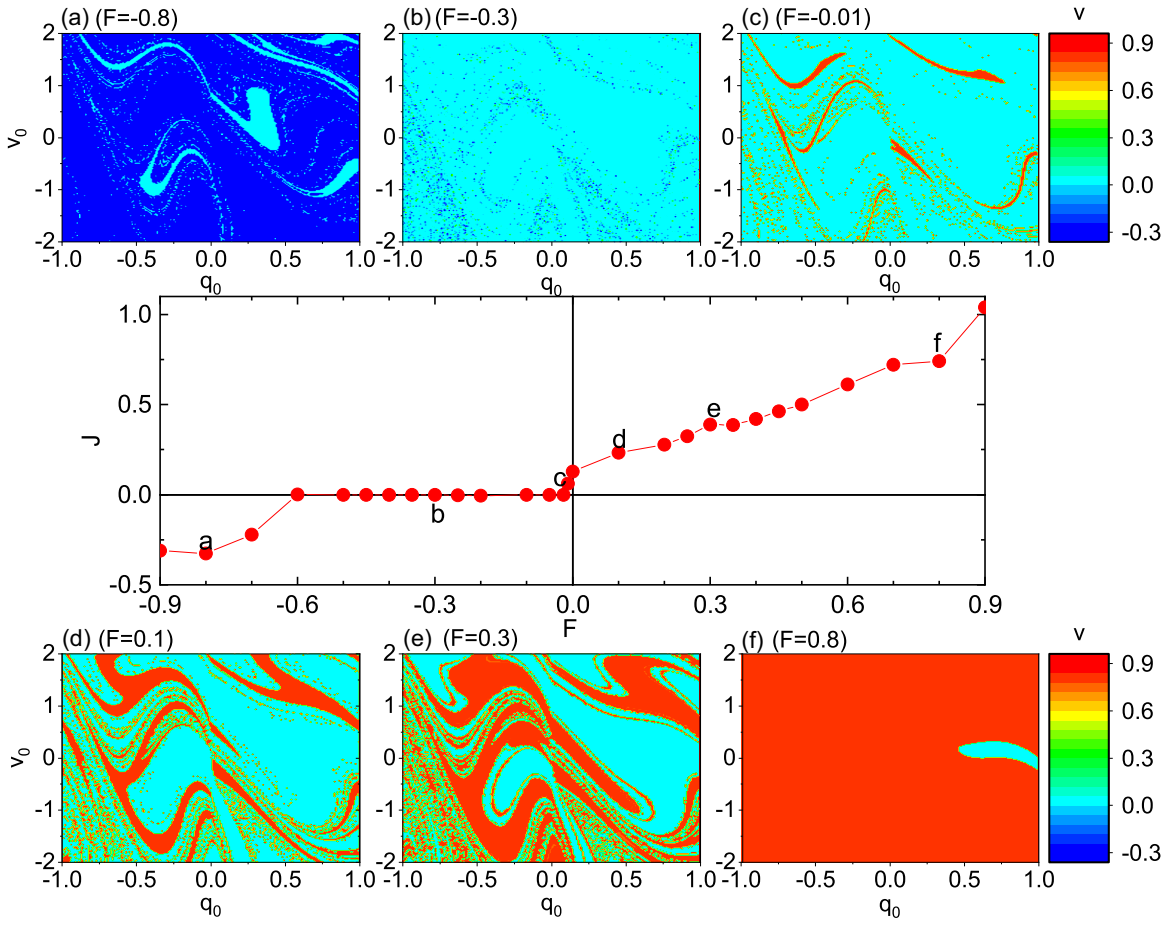

FIG. 1. The flux of the particle vsersus the bias (the middle row), and the basins of attraction for $F = -0.8$ (a), -0.3 (b), -0.01 (c), 0.1 (d), 0.3 (e), and 0.8 (f). The other parameters are $\gamma_r = 0.7$ and $\lambda = 0.2$.

where p and q denote the momentum and position of the Brownian particle, respectively. $\mathfrak{F}(t)$, the driving forces, is given by $\mathfrak{F}(t) = -F - A\sin(\omega t)$, where F is an external constant bias to manipulate the rectification and $A\sin(\omega t)$ is an external time-periodic force with amplitude A and frequency ω to drive the system far away from an equilibrium state. Thus the motion of the particle follows the equations of motion [58]

$$\frac{dq}{dt} = \frac{\partial H}{\partial p} = \frac{p}{m},$$
$$\frac{dp}{dt} = -\frac{\partial H}{\partial q} - \gamma(q)p, \tag{2}$$

where $\gamma(q)p$ is damping term. Here $\gamma(q)$ is the position-dependent friction coefficient. Namely, it is strongly correlated with the potential barrier, implying that different potential barriers have different friction coefficients. For example, a recent work [61] demonstrated that the periodic potential adds the escape time that a particle needs to leave a potential well. This may mean that different potential barriers possess different friction coefficients. Thus the friction coefficient is given by $\gamma(q) = \gamma_l$ for $q < 0$, while $\gamma(q) = \gamma_r$ for $q \geqslant 0$.

We fix $m = 1.0$, $U_l = 1.0$, $A = 4.2$, $\omega = 4.9$, and $\gamma_l = 0.9$, unless otherwise stated. All quantities are in dimensionless units. We here investigate the flux and the corresponding basin of attraction in the system via numerical simulation. To obtain more credible results, here we numerically solve Eq. (2) using the fourth-order Runge-Kutta integrator with a typical time step of $\Delta t = 10^{-3}$. The initial positions $q(t = 0)$ and velocities $v(t = 0)$ of the particle are uniformly distributed between -1.0 and 1.0 and between -2.0 and 2.0, respectively. We remove the 10^6 data of initial transient state and then employ 10^7 data of the steady state to calculate the flux of the particle.

Figure 1 shows the flux of the particle as a function of the bias and the basins of attraction corresponding to $F = -0.8$, -0.3, -0.01, 0.1, 0.3, and 0.8. Here we define the flux of the particle as $J = \langle v \rangle / L$ [20,62], where $\langle v \rangle$ denotes the average velocity of the particle and L is the period of the potential. Here L is equal to 1, and thus we obtain $J = \langle v \rangle$. The forward flux J_+ denotes the flux of the particle that jumps from the initial positions to the right substrate potential with the low potential barrier for the positive bias ($F > 0.0$). The reverse flux J_- represents the flux of the particle that moves from the initial positions to the left substrate potential with the high potential barrier for the negative bias ($F < 0.0$). Namely, the average velocity corresponding to $F > 0$ is J_+, and it is J_- for $F < 0$. Figure 1 shows that the threshold biases F_{th} are -0.02 and -0.6 for the appearance of $J_+ \neq 0$ and $J_- \neq 0$, respectively. In the absence of F, $J \neq 0$ reveals the appearance of the ratchet effect. Moreover, upon further increasing F above F_{th}, the magnitude of J_+ is larger than that of J_-

for the identical magnitudes of the bias. Therefore, these findings reveal that there exists a rectification of the flux in the system.

Next, we attempt to explain these results via the basin of attraction, which was used to interpret the anomalous transports of the particle in recent works [63,64]. At $F = -0.8$, the system shows that there are two different stable basins of attraction, denoted by the cyan and blue in Fig. 1(a). Here the cyan represents the running states with velocity $v \simeq 0.02$, while the blue is the running state with velocity $v \simeq -0.35$. Therefore, the average velocity is negative because of the existence of small cyan basins and large blue basins. This result is in agreement with the result obtained from directed calculation. Interestingly, for small initial velocities, a trivial wrinkle occurs at $q_0 = 0.0$ due to the existence of different potential barriers. For $F = -0.3$, Fig. 1(b) shows that there exists a superstable cyan basin. And other unstable regimes are mixed states, including both positive and negative velocities. Therefore, the average velocity is nearly zero and consistent with that of directed simulation. This result can be interpreted as follows. With the increase of F, the blue basin gradually loses its stabilities, and the cyan basin becomes more stable. At $F = -0.01$, Fig. 1(c) shows that besides the existence of the cyan basin, a new basin, denoted by red, appears. Here the red denotes the running state with velocity $v \simeq 0.79$. Therefore, the average velocity is positive for the existence of the stable basins corresponding to positive velocities only. This finding is in agreement with the result obtained via directed numerical simulation. Because of the presence of different substrate potentials at $q_0 = 0.0$, there exists a nontrivial wrinkle for small initial velocities.

Now consider a positive load driving the system, how it affects the flux. For $F = 0.1$, Fig. 1(d) exhibits that there exist two different stable basins: the red basin and the cyan basin. Thus the average velocity is positive for the existence of the basin of attraction corresponding to positive velocities. Notice that the red basins for $F = 0.1$ are larger than those for $F = -0.01$, whereas the blue basins for $F = 0.1$ are smaller than those for $F = -0.01$, implying that the average velocity for $F = 0.1$ is larger than that for $F = -0.01$. Moreover, the different potential barriers at $q_0 = 0.0$ result in the occurrence of a nontrivial wrinkle. Figure 1(e) shows that the red basins for $F = 0.3$ are larger than those for $F = 0.1$, whereas the cyan basins for $F = 0.3$ are smaller than those for $F = 0.1$. Furthermore, a nontrivial wrinkle also occurs at $q_0 = 0.0$. For $F = 0.8$, it is clear from Fig. 1(f) that there exists a large red basin and a trivial cyan basin. It is noteworthy that the wrinkle vanishes at $q_0 = 0.0$. Notice that the structures of basins of attraction for $F = -0.3$ and -0.8 are different from those for $F = 0.3$ and 0.8, respectively. These findings suggest that J_- for $F = -0.3$ and -0.8 are not equal to J_+ for $F = 0.3$ and 0.8, respectively. In a word, the basin of attraction can lead to J_+ not being equal to J_- in the system.

To gain more insight into the rich dynamical behaviors, we present the corresponding phase-space map and power spectrum density in Appendix A. Phase-space maps exhibit that with identical system parameters, different initial conditions lead to different dynamical phenomena. The power spectrum densities also demonstrate these phenomena. Namely, these findings suggest that the dynamical behaviors are very insensitive to the initial conditions. Therefore the unpredictability of the physical system may depend on the initial condition.

III. THE STOCHASTIC MODEL

We now turn to the system with a thermal noise. Due to the presence of thermal noise, the particle is a Brownian particle. It is described by the Langevin equation of the form [58]

$$\frac{dq}{dt} = \frac{\partial H}{\partial p} = p,$$
$$\frac{dp}{dt} = -\frac{\partial H}{\partial q} - \gamma(q)p + \xi(t), \tag{3}$$

where $\xi(t)$ denotes thermal noise modeled by a Gaussian white noise of zero mean with the property $\langle \xi(t)\xi(t')\rangle = 2\gamma_i k_B T \delta(t-t')$. Here γ_i is γ_l for $q < 0$ and γ_r for $q \geqslant 0$, and k_B and T denote the Boltzmann constant and temperature, respectively. Equation (3) is integrated using the second Runge-Kutta algorithm [65] with the time step $h = 10^{-2}$. We also employ the Verlet algorithm to discretize Eq. (3) and obtain the identical results. Initial positions $q(t=0)$ and velocities $v(t=0)$ of the particle are both uniformly distributed between -1.0 and 1.0. To guarantee sufficient convergence of the result of the flux, we perform simulations over 10^7 time steps and with up to 500 trajectories. Moreover, the 10^6 data of initial transient states are removed, and 10^7 data are then used to compute the average velocity. Furthermore, the time-dependent diffusion coefficient (TDC) is defined by $D(t) = \langle \Delta x^2(t)\rangle/(2t)$ [66], where $\langle \Delta x^2(t)\rangle = \langle x^2(t)\rangle - \langle x(t)\rangle^2 \propto t^\beta$ denotes the mean-squared displacement (MSD). Here $\langle\cdot\rangle$ denotes the ensemble average of 10^4 trajectories. Notice that $D(t) = \text{const}$ denotes normal diffusion, the increase of $D(t)$ with time denotes superdiffusion, and the decrease of $D(t)$ with time denotes subdiffusion. In addition, $\beta < 1$ is subdiffusion, $\beta = 1$ is normal diffusion, $\beta > 1$ is superdiffusion, $\beta = 2$ is ballistic diffusion, and $\beta > 2$ is hyperdiffusion. Finally, we also study the corresponding IE, which is defined by $S = \sum -P(v_i)\log[P(v_i)]$ [42,43], where $P(v_i)$ denotes the probability distribution of the particle's velocities. Here we mainly focus on the rectification of the flux and the corresponding diffusion and IE of the particle.

To quantify the TDC and IE corresponding to the rectification, let S_+ and $D_+(t)$ denote the IE and TDC corresponding to J_+, respectively. S_- and $D_-(t)$ represent the IE and TDC corresponding to J_-, respectively. How then can we characterize the rectification of the systems in an efficient way? Surely it is the rectifying efficiency that is given by $R = |J_+|/|J_-|$ [6]. Notice that there is no rectification for $R = 1$, while $R \simeq \infty$ is a perfect rectification. To obtain more insight into the characteristics of the rectification, we also compute the rectification coefficient. It is well known that the rectifying efficiency is multiple orders of magnitude, thus the rectification coefficient cannot well characterize the rectification. However, the rectification coefficient can explicitly provide the signals of whether or not the rectification is negative. It is given by [67]

$$C = \frac{|J_+| - |J_-|}{|J_+| + |J_-|}. \tag{4}$$

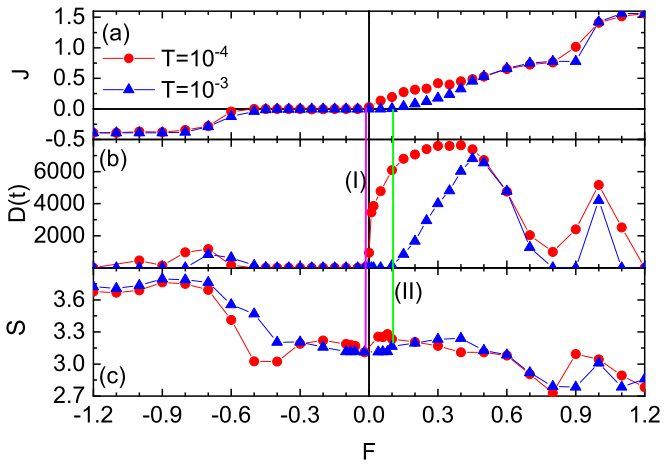

FIG. 2. The flux of the particle (a), the corresponding TDC $D(t)$ with $t = 10^5$ (b), and the corresponding IE S (c) vs the bias for different temperatures. The other parameters are $\lambda = 0.2$ and $\gamma_r = 0.7$.

Notice that $C = 0$ denotes that there is no rectification, and $C > 0$ and <0 represent positive rectification and negative rectification, respectively. Moreover, there is a perfect particle rectification for $C = \pm 1$.

To study the emergence of rectification in the system with thermal noise, we consider the flux of the particle as a function of F for different T in Fig. 2(a). It shows that for $T = 10^{-4}$, the threshold biases F_{th} are nearly 0.0 and -0.5 for the appearances of $J_+ \neq 0$ and $J_- \neq 0$, respectively. For $T = 10^{-3}$, the threshold biases F_{th} are 0.1 and -0.45 for the existence of $J_+ \neq 0$ and $J_- \neq 0$, respectively. Notice that for $F = 0.0$, the flux is nonzero for $T = 10^{-4}$ and zero for $T = 10^{-3}$, revealing that the thermal noise weakens or eliminates the ratchet effect. With increasing F above F_{th}, Fig. 2(a) shows that the magnitude of J_+ is larger than that of J_- for the identical magnitude of the biases. These results reveal that there exists a rectification of the flux in the system. Having the behavior of this rectification, the system becomes a perfect diode of the flux of the Brownian particle.

Moreover, Fig. 2(b) shows the TDC $D(t)$ with $t = 10^5$ as a function of F. It is well known that for a certain time interval, the diffusion may be normal, ballistic, subdiffusive, or superdiffusive for different system parameters. Namely, different parameters correspond to different types of diffusions for the identical time interval. Therefore, we study TDC $D(t)$ instead of the effective diffusion coefficient here. For $T = 10^{-4}$, Fig. 2(b) shows that no diffusion occurs for F ranging from 0.0 to -0.5 [namely, $D_-(t) \simeq 0.00$], and there exists a trivial diffusion for F ranging from -0.5 to -0.9. Contrarily, TDC $D_+(t)$ is nontrivial for F ranging from 0.0 to 0.5, and $D_+(t)$ for F ranging from 0.5 to 0.8 is generally larger than $D_-(t)$ for F ranging from -0.5 to -0.8. The curve of $D(t)$ corresponding to $T = 10^{-3}$ is similar to that corresponding to $T = 10^{-4}$. It is also shown that $D(t)$ corresponding to $T = 10^{-3}$ is generally smaller than that corresponding to $T = 10^{-4}$. Notice that the flux corresponding to $T = 10^{-3}$ is also almost smaller than that corresponding to $T = 10^{-4}$. These behaviors suggest that the rectification may be correlated with the diffusion in the system. Actually, MSD denotes the uncertainty of the position for the particle, implying that the larger the TDC is, the larger the uncertainty of position is. Therefore, the uncertainty decreases with the increase of a large bias due to the decrease or disappearance of the effect of the potential, thus the system is an ordered system [e.g., $F = 1.2$ in Fig. 2(b)].

We now turn to the corresponding IE. Figure 2(c) shows the IE S as a function of the bias for different T. For $T = 10^{-4}$, there exists a minimum at $F \approx 0.0$, in which the drastic transitions of diffusion, flux, and IE arise. As illustrated in the label I, there are transitions from no flux to a finite net flux, from no diffusion to a nontrivial diffusion, and from a small IE to a large IE. The identical behavior arises for $T = 10^{-3}$, as shown in the label II. Furthermore, the figure displays that there are two relative minima at $F = -0.5$ and $F = 0.8$. As the magnitude of F further increases, the fluxes and diffusions increase, too. The increase of IE S with the increasing F implies that the system becomes more disordered in the nonlinear response regimes. Then S decreases with further increasing F, implying that the transition from the nonlinear response to the linear response regime appears [68]. Namely, the system becomes ordered. It should be also noted that the entropy S_+ for F is not equal to S_- for $-F$. For J_+, the particle moves from the initial positions to the low substrate potential of the right, whereas it moves from the initial positions to the high substrate potential of the left for J_-. Therefore the system for J_+ reaches the linear response regime earlier than that for J_- with increasing driving force. This leads to the appearance of the rectification of the flux.

Based on these findings, we find that the region of $J \approx 0.0$ almost corresponds to that of the diffusion $D(t) \simeq 0.0$ and of the relatively small entropy S (e.g., F from 0.0 to -0.5) for small biases. While the regimes of $J \neq 0$ correspond to those of the diffusion $D(t) > 0.0$ and of the increasing entropy S in the nonlinear response regime or decreasing entropy S in the quasilinear response regime. These results suggest that the diffusion corresponding to J_+ is not identical to that corresponding to J_- for the identical magnitude of the biases since one may be in the linear response regime and the other may be in the nonlinear response regime. Moreover, IEs show that the former may be ordered whereas the latter may be disordered. The possible reasons for these findings will be analyzed below.

To understand the rectification in the system with a thermal noise, we next discuss the dependence of the rectification and its statistical properties of the particle on the temperature T. As shown in Fig. 3, we present J_+, J_-, $D_+(t = 10^5)$, $D_-(t = 10^5)$, S_+, S_-, R, and C vs T for different F.

Figure 3(a) shows that for $|F| = 0.13$, J_+ has a minimum with increasing T and is larger than J_- at low and high temperatures, suggesting that the rectification of the flux arises in these ranges [e.g., $T < 10^{-3}$ and $T > 10^{-2}$ in Fig. 3(a)]. However, they are almost equal to each other in a certain range (e.g., $T = 10^{-3}$), implying that the rectification disappears. To understand this finding, we present the corresponding TDC $D(t)$ with $t = 10^5$ as a function of T in Fig. 3(e). At low temperature (e.g., $T < 10^{-3}$), $D_+(t)$ is lager than $D_-(t)$. As T increases (e.g., $T = 10^{-2}$), $D_+(t)$ is smaller than $D_-(t)$ in Fig. 3(e). Upon further increasing T, $D_+(t)$ is lager than $D_-(t)$

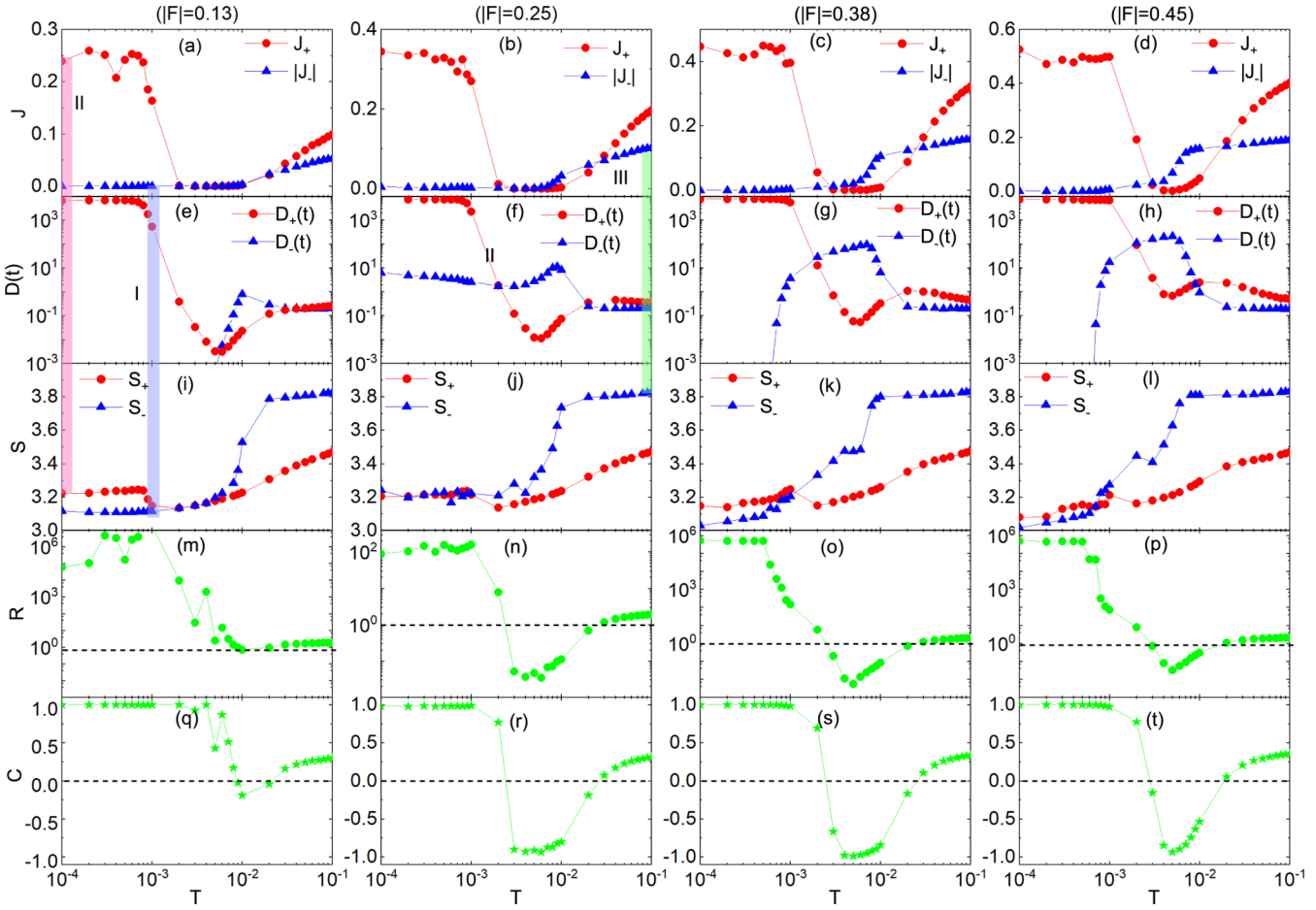

FIG. 3. The flux of the particle (the first row), TDC $D(t)$ with $t = 10^5$ (the second row), IE S (the third row), rectifying efficiency (the fourth row), and rectification coefficient (the fifth row) vs the temperature T for $|F| = 0.13$ (the first column), 0.25 (the second column), 0.38 (the third column), and 0.45 (the fourth column). The other parameters are $\gamma_r = 0.7$ and $\lambda = 0.2$.

again. The changes of $D(t)$ with $t = 10^5$ are almost identical to those of J. The IEs S_+ and S_- as functions of T in Fig. 3(i), showing that at low temperature, S_+ is larger than S_-. As T increases, they are equal to each other. At high temperature, the S_+ is smaller than S_-, implying that the system for J_- is more in disorder than that for J_+. Moreover, the varying temperature leads to a transition from several to 10^5 times of rectifying efficiency [Fig. 3(m)], implying that it can tune the rectification [Fig. 3(q)].

For $F = 0.25$, J_+ is larger than J_- for a low- or high-temperature T (e.g., $T = 10^{-4}$ or 10^{-1}) in Fig. 3(b). However, an unexpected phenomenon occurs that J_- is larger than J_+ for T ranging from 2×10^{-3} to 10^{-2}. This finding implies that the rectifying efficiency R is smaller than 1 [Fig. 3(n)] and the negative rectification appears. Namely, there exists a rectification in the opposite direction, as shown in Fig. 3(r), displaying that the rectification coefficient is negative. This phenomenon is similar to the reversible diodes for moving quanta [1]. This finding demonstrates the emergence of a negative rectification for the Brownian particle. Notice that the negative rectification had been investigated extensively in the current [53–56] and the thermal flux [57]. Additionally, it should be noted that the variation of TDC $D_+(t)$ with varying temperature in Fig. 3(f) matches that of the flux with changing temperature in Fig. 3(b). Namely, the $D_+(t)$ is larger than $D_-(t)$ in low or high temperature, whereas the $D_+(t)$ is smaller than $D_-(t)$ for T ranging from 2×10^{-3} to 10^{-2}, as shown in Fig. 3(f). Figure 3(j) shows for T in this range, that S_+ is smaller than S_-, meaning that the system for J_- is in more disorder than that for J_+.

The results of the flux, diffusion, and entropy with varying T for $|F| = 0.38$ and 0.45 are similar to those for $|F| = 0.25$, as shown in Figs. 3(c), 3(d), 3(g), 3(h), 3(k), and 3(l). The difference is that as F increases, the negative rectification increases first and then decreases. This behavior also shows in the rectifying efficiency R and the rectification coefficient C, as shown in Figs. 3(o), 3(p), 3(s), and 3(t). These phenomena can be well interpreted by MSD and TDC in Appendix B. In brief, the thermal noise can weaken or eliminate the rectification of the system, and the combination of the bias and noise can lead to negative rectification.

We now turn to a kinetic phase transition for these findings. Figures 3(a)–3(d) show that at $T \simeq 10^{-3}$, J_+ drops sharply near zero, suggesting that these exits a kinetic phase transition from a finite net transport to no transport [45–47] through the variation of the temperature. Surely it is of the second order. It is noteworthy that the corresponding $D_+(t)$ also drops sharply (over four orders of magnitude) for $T \simeq 10^{-3}$. Additionally, the corresponding S_+ shows that there exists a drop, revealing that a phase transition of the IE arises too [69]. Therefore, for

TABLE I. The relationship among IE, TDC, flux, etc.

Entropy	TDC $D(t)$	Symmetry of $p(v)$ at $v=0$	Flux	System	Case
Small	Small	Yes	Zero	Disordered	I
Small	Large	No	Nonzero	Disordered	II
Large	Small	No	Nonzero	Disordered	III
Small	Small	No	Nonzero	Ordered	IV

forward flux, a phase transition appears at $T \simeq 10^{-3}$. Furthermore, when T ranges from 5×10^{-3} to 10^{-2}, both J_+ and J_- show that there exists another kinetic phase transition from no transport to a finite net transport. S_+ and S_- also demonstrate the existence of the phase transition. The diffusion coefficients correspond to a dramatic change in the regime. Finally, it should be noted that the negative rectification arises in the range between double phase transitions for the forward flux. In brief, multiple kinetic phase transitions, resulting from the variation of the temperature, can result in negative rectification and anomalous diffusion.

To find the underlying mechanism corresponding to the findings of Fig. 3, we analyze them via MSD, TDC, and the probability distribution of the velocity in Appendix B. For J_+, the diffusion is ballistic at low temperature and normal at high temperature. On the other hand, for J_-, the diffusion disappears at low temperature and is normal at high temperature. Unexpectedly, for certain parameters, diffusion is subdiffusive first, then becomes superdiffusive and finally normal. Namely, the types of diffusions are different for different time intervals. The probability distribution of the velocity is non-Gaussian at low temperature, meaning that the diffusion is anomalous. At high temperature, the distribution is close to a Gaussian distribution, implying that the diffusion is normal. In a word, the diffusions for the forward flux are different those for the reverse, and they are anomalous at low temperature.

To address the issue of how the bias influences the rectification, we plotted the fluxes, TDCs, IEs, rectifying efficiency, and rectification coefficient versus the bias in Appendix C. Those results show that the rectification is sensitive to the bias, therefore it can tune the rectification. Additionally, we compared the forward and reverse fluxes for different T, which shows that the lower the temperature is, the wider the parameter range of rectification is. Furthermore, the diffusions are anomalous at low temperature and normal at high temperature. The probability distributions of the velocity also prove these findings. In brief, the findings also show that the thermal noise can suppress the rectification in Brownian motion.

These findings mentioned above are summarized in Table I, which shows that there exit four cases. For $T = 10^{-3}$, J_-, $D_-(t)$ with $t = 10^5$, and S_- for $F = -0.13$ are small, and the corresponding distribution of the velocity with both negative and positive velocities, which is presented in Appendixes B and C, is symmetric around $v = 0.0$. Thus the system may be disordered. The case is called I in Table I, labeled "I″ in Fig. 3, which suggests that the particle may stay in the initial well. At $T = 10^{-4}$, J_+ and $D_+(t)$ with $t = 10^5$ for $F = 0.13$ are large, the corresponding S_+ is small, and the corresponding probability distribution of the velocity with both negative and positive velocities is asymmetric around $v = 0.0$. Therefore the system may be disordered. This case is called II in Table I, as shown in Fig. 3. The third case is labeled "III" in Fig. 3, which shows that S_- is larger, $D_-(t)$ with $t = 10^5$ is small, the flux is larger, and the probability distribution with negative and positive velocities is asymmetric around $v = 0$. It is listed in Table I, labeled "III." The last case is labeled "IV" in Appendix C (Fig. 10). It shows that for $F = 0.45$, S_+ and $D_+(t)$ with $t = 10^5$ (it is smaller than 1.0) is small, the flux is nontrivial, and the probability distribution shows only positive velocity. Thus the system is ordered. It is called "IV" in Table I, which shows that the system is in the linear response regime. Except for the cases of no flux and the ordered system, other cases show that when the IE is small, the TDC $D(t)$ is large, and vice versa. It should be also noted that the asymmetry of the probability distribution around $v = 0$ leads to the appearance of the flux. Based on the presence of the flux, the diffusion and IE corresponding to J_+ are not equal to those corresponding to J_- due to a system with different potential barriers, which results in the existence of the rectification.

To generalize the results and make them suitable for experimental validation, we present 2D maps of J_+, J_-, $D_+(t = 10^5)$, $D_-(t = 10^5)$, S_+, and S_- as functions of γ_r and λ in Fig. 4. Their magnitudes are indicated with corresponding color codes. Figures 4(a) and 4(b) show that for most of the parameter ranges, J_+ are not equal to J_-, suggesting that there exits rectification in these parameter regimes. For example, there is red in Fig. 4(a) whereas it is not in Fig. 4(b) for the same parameter regimes. Moreover, in certain parameter regimes, the colors of J_+ in Fig. 4(a) are the same as those of J_- in Fig. 4(b), such as the yellow regime, indicating the disappearance of the rectification. However, in certain parameter regimes, J_- are larger than J_+, such as the blue and cyan regimes in Fig. 4(a) corresponding to the light green and yellow regimes in Fig. 4(b). This suggests that negative rectification occurs in these regimes. Additionally, the rectification disappears when the potential barrier and friction coefficient of the right are equal to those of the left, as shown in the top right corner of Figs. 4(a) and 4(b).

Let us now consider the corresponding diffusion, which is presented in Figs. 4(c) and 4(d). The diffusion shows that for most of the parameter regimes, the cyan and blue regimes in Fig. 4(c) correspond to the green regimes in Fig. 4(d), and the cyan in Fig. 4(c) corresponds to the red in Fig. 4(d). These findings suggest that $D_+(t)$ are smaller than $D_-(t)$ in these regimes. Moreover, in certain parameter regimes, the green regimes in Fig. 4(c) correspond to the green regimes in Fig. 4(d). This implies that $D_+(t)$ are equal to $D_-(t)$. We also find that when the potential barrier and friction coefficient of the right are equal to those of the left in the top right corner, $D_+(t)$ is also equal to $D_-(t)$. This means that the rectification vanishes. In other words, the $D_+(t)$ are not equal to $D_-(t)$ when the potential barrier and friction coefficient of the left are not equal to those of the right, and this may lead to rectification.

The corresponding S is presented in Figs. 4(e) and 4(f). We find from that for a small λ (e.g., $\lambda < 0.1$), the blue parameter regimes in Fig. 4(e) correspond to the deep red parameter

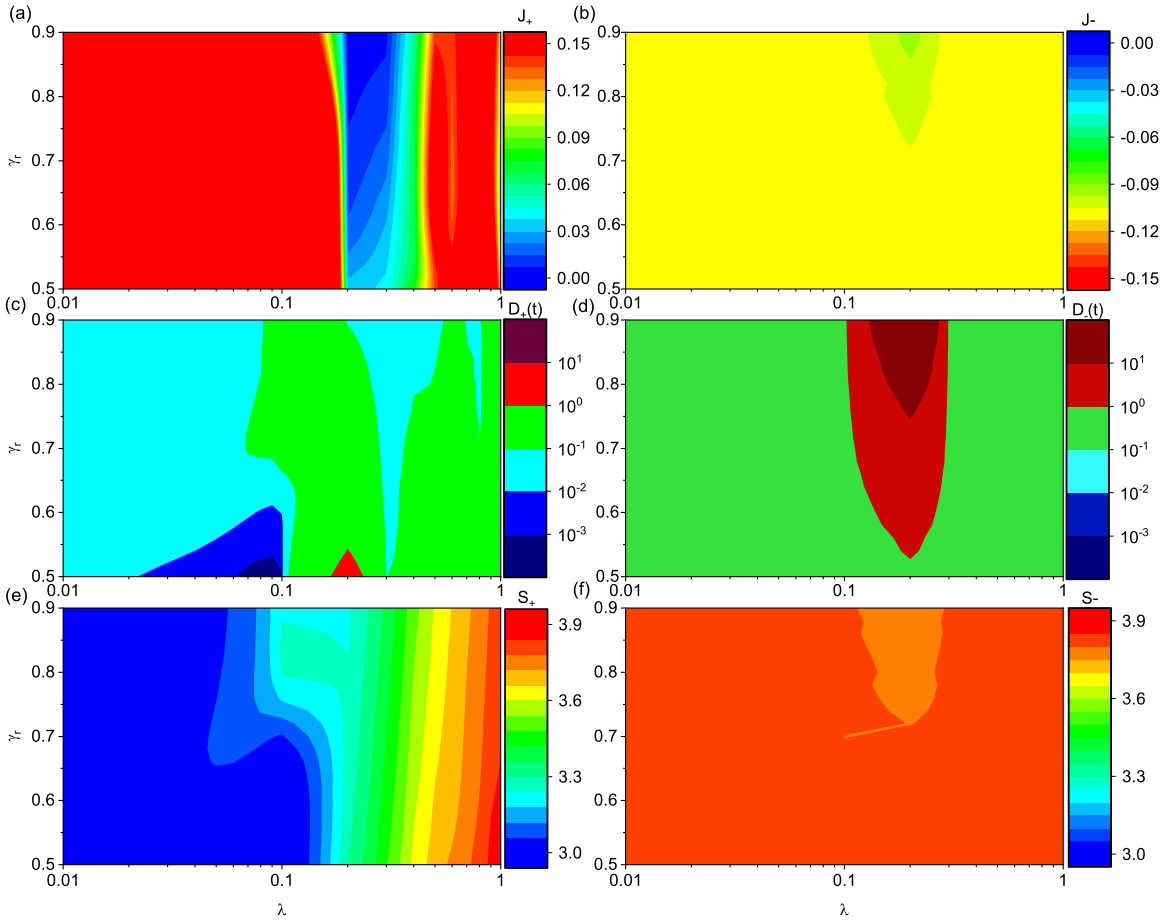

FIG. 4. Two-dimensional map of the forward flux J_+ (a), reverse flux (b), $D_+(t)$ with $t = 10^{-5}$ (c), $D_-(t)$ with $t = 10^{-5}$ (d), S_+ (e), and S_- (f) as functions of the friction coefficient γ_r and the parameter λ. The other parameters are $T = 10^{-2}$ and $F = 0.38$.

regimes in Fig. 4(f). Namely, S_+ is smaller than S_-, implying that the system for the forward flux is more ordered than that for the reverse and there exists the rectification. For a large λ, however, S_+ is almost equal to S_-, suggesting that the rectification vanishes.

By comparison, we find that the changes of the maps of $D_+(t)$ in Fig. 4(c) and S_+ in Fig. 4(e) are similar to those of J_+ in Fig. 4(a), while the changes of the maps of $D_-(t)$ in Fig. 4(d) and S_- in Fig. 4(f) are similar to those of J_- in Fig. 4(b). J_+ corresponding to F is not equal to J_- corresponding to $-F$ due to different potential barriers and friction coefficients. Moreover, $D_+(t)$ and S_+ are not equal to $D_-(t)$ and S_- as well, respectively. For $\lambda < 0.05$, the particle moves in the ordered system when it moves from initial positions to the right substrate potential with the low potential barrier, thus the forward fluxes are nontrivial in Fig. 4(a). Moreover, the corresponding $D_+(t)$ and S_+ are trivial in Figs. 4(c) and 4(e), implying that the system is ordered. On the contrary, for $\lambda < 0.05$, the particle moves in nonlinear response regimes when it moves from the initial positions to the left substrate potential with the high potential barrier, and the system is disordered. Thus J_- in Fig. 4(b) are smaller than the corresponding J_+ in Fig. 4(a). Additionally, both $D_-(t)$ and S_- are larger than $D_+(t)$ and S_+, respectively, as shown in Figs. 4(c), 4(d), 4(e), and 4(f).

For $0.05 < \lambda < 0.4$, J_+ of certain parameter regimes are nontrivial [the red regimes in Fig. 4(a)], the corresponding TDC $D_+(t = 10^5)$ are also nontrivial [the red regimes in Fig. 4(c)], and the corresponding S_+ are larger than those for $\lambda < 0.05$ [the cyan regimes in Fig. 4(c)]. Moreover, in other parameter regimes, J_+ are trivial [e.g., the blue regime in Fig. 4(a)], the corresponding $D_+(t)$ are trivial [e.g., the green and cyan regimes in Fig. 4(c)], and the corresponding S_+ are indicated with the green, yellow, and cyan in Fig. 4(e). On the other hand, J_- are trivial in Fig. 4(b), and S_- in this regime are smaller than those of the other regimes in Fig. 4(f), whereas $D_-(t)$ in this regime are larger than those of the other regimes.

Finally, for $\lambda > 0.4$, J_+ are nontrivial in Fig. 4(a), and $D_+(t)$ are trivial in Fig. 4(d), whereas S_+ in this regime are larger than those of other regimes in Fig. 4(e). Contrarily, J_- are trivial in Fig. 4(b), and $D_-(t)$ are also trivial in Fig. 4(d), whereas S_- are nontrivial in Fig. 4(f). These results can be summarized as follows. In the linear response regime, the larger the flux is, the smaller the TDC and IE are. In the nonlinear response regime, however, the flux depends on the diffusion and entropy, which the TDC is trivial whereas IE is nontrivial, and vice versa.

We now turn to a kinetic phase transition. Figure 4(a) shows that for fixed γ_r, there exist double kinetic phase transitions between finite net transport and no transport through

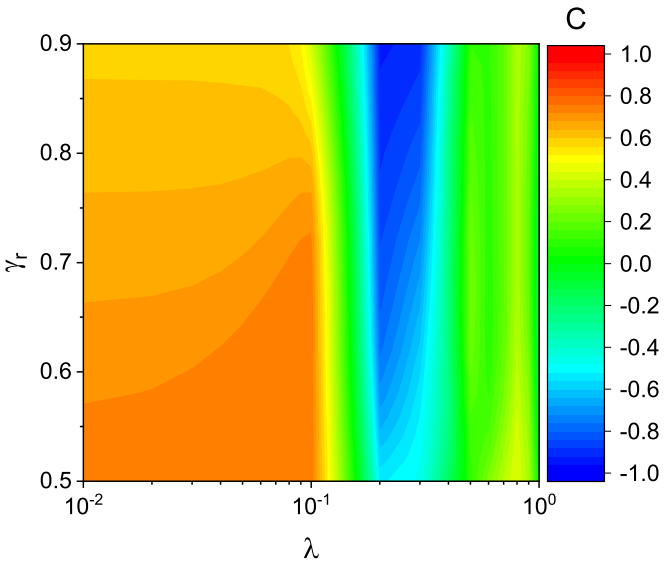

FIG. 5. Two-dimensional map of rectification coefficient as a function of the friction coefficient γ_r and the parameter λ. The other parameters are $T = 10^{-2}$ and $F = 0.38$.

the variation of the parameter λ. The IE also shows that there are phase transitions via the change of the parameter λ in Fig 4(e). The negative rectification arises in the range between double kinetic phase transitions, as shown in Fig. 5. Therefore the parameters λ and γ_r play a key role in tuning negative rectification.

Figure 5 shows the map of rectification coefficient C as a function of γ_r and λ. The color code denotes a corresponding magnitude of the rectification coefficient. The orange and yellow represent $C \simeq 0.7$ and 0.5, respectively, suggesting that a large rectification arises in these parameter ranges, whereas the blue denotes $C \simeq -1$, implying that perfect negative rectification occurs in the parameter ranges. Moreover, the green indicates $C \simeq 0$, revealing that no rectification occurs in those parameter ranges. In brief, with those tailored parameters read off from Fig. 5, we can tune the rectification coefficient to the orange, yellow, or blue regimes of friction coefficient γ_r by varying the parameter λ at a fixed periodic driving strength. Therefore, the combination of these parameters can tune a perfect rectification.

IV. RECTIFICATION OF INTERACTING BROWNIAN PARTICLES

We now turn to the interacting particles moving in the system. It is described by the Hamiltonian

$$H = \sum_{i=1}^{N}\left[\frac{p_i^2}{2m_i} + U(q_i)\right] + U_{int}(q) + \sum_{i=1}^{N}\mathfrak{F}(t)q_i, \quad (5)$$

where $U_{int}(q) = \sum_{i=1}^{N} K\ln(q)$ denotes the potential of the interacting particles, and N is the number of the interacting particles. Thus, the interacting force is obtained by [70] $F(q_i) = -\frac{\partial U_{int}(q_i)}{\partial q_i} = \sum_{j\neq i}\frac{K}{q_i - q_j}$, where K is the coupling strength between interacting particles. The method of the numerical simulation is the same as that of Sec. III.

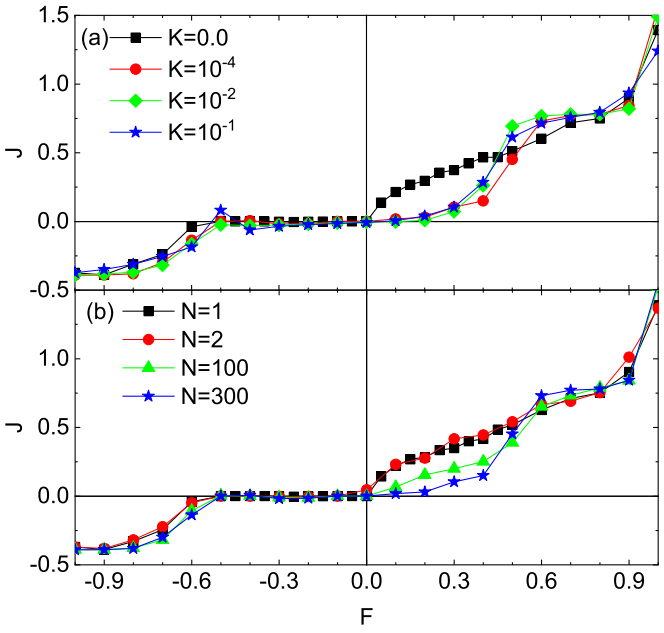

FIG. 6. The flux of the interacting particles vs the bias for different coupling strengths K (a) and number of the particles N (b). The other parameters are $\gamma_r = 0.7$, $\lambda = 0.2$, $T = 10^{-4}$, $N = 300$ for (a) and $K = 1.0$ for (b).

The results of the interacting Brownian particles are presented in Fig. 6. Figure 6(a) shows the flux as a function of the bias for different coupled strengths K. We find that different coupling strengths lead to different threshold values of the bias for the emergence of the forward flux and may cause different magnitudes of the fluxes for the identical bias. Unexpectedly, for certain parameter regimes, the magnitudes of the fluxes do not change with increasing F. This behavior does not arise for a single particle, no interaction particles, the weak coupling between particles, or the reverse flux of interacting particles. This phenomenon may imply that the collective motion appears for the interacting particles. Part of this phenomenon also arises for different numbers of interacting particles, as shown in Fig. 6(b). Namely, different numbers of the interacting particles result in different fluxes and threshold values of the bias for the emergence of the forward flux. Therefore these findings suggest that coupling strengths or the number of interacting particles can weaken or enhance the rectification in the system. Namely, for different coupling strengths or the number of interacting particles, the threshold values of the biases may be different. In certain parameter regimes, the flux is almost a constant with the varying bias.

V. CONCLUSION

In conclusion, we numerically investigate the Brownian particles moving in the system driven by an external bias and an external time-dependent force for the deterministic case and the presence of thermal noise. The system consists of two components which have identical shapes and different potential barriers with different friction coefficients. It is noteworthy that a system with different materials is

extensively used to tune the transport of various particles, e.g., electron transport in a diode, rectification switching in ruthenium-complex molecular junctions [4], phonons in different substrate potentials [7], etc. We also study the transport of the interacting particles in the system.

We focus on the rectification of the flux of the Brownian particle in the system. The deterministic system exhibits perfect rectification of the flux and the ratchet effect. Interestingly, the relationship between the flux and the bias is similar to that between the voltage and the electronic current [21] or between the temperature and heat flux [6,23]. To understand the rectification, we analyze the phenomenon via the basin of attraction and ask the question of how does it affect the rectification. It is shown that the unpredictability of dynamics depends on the initial positions and velocities of the particle, and that there exists a wrinkle in the basin of attraction arising from the system with different potential barriers.

For the system with a thermal noise, we present the forward and the reverse fluxes with varying the temperature and the driving force. The system exhibits that there also exists the rectification of the fluxes for the Brownian particle, and the ratchet effect is eliminated at high temperature. We also give the corresponding rectifying efficiency and rectification coefficient as well. The forward flux reveals that there exists a kinetic phase transport from a finite net transport to no transport with the increase of the low temperature. Additionally, both forward and reverse fluxes exhibit that there exists a kinetic phase transition from no transport to a finite net transport with the increase of the high temperature. Unexpectedly, the negative rectification arises in the range between two kinetic phase transitions for the forward flux. That is, for the identical magnitudes of the biases, the particle cannot jump from the initial well to the right substrate potential with low potential barrier but moves from the initial well to the left substrate potential with the high potential barrier. To better understand the phenomena, we also investigate the corresponding TDC and IE. We interpret these results with MSD, TDC, and probability distribution of the velocity in the Appendixes. At low temperature, the system exhibits normal diffusion, subdiffusion, superdiffusion, and ballistic diffusion, whereas diffusion is normal only at high temperature.

To generalize the results obtained by our model and make them suitable for experimental validation, we present the selected parameter regimes in which the rectification of flux arises through the maps of the forward and reverse fluxes, TDCs, and IEs. These results suggest that in an ordered system, the larger the flux is, the smaller TDC and IE are. However, for the emergence of the flux in a disordered system, the larger the TDC is, the smaller IE is in certain parameter regimes, and vice versa. For no transport, both TDC and IE are small or large. Namely, the particle always remains in the initial well during the time evolution. We can tune the rectification coefficient to the best parameter regime with the map of the rectification coefficient.

Finally, we also study the rectification of the interacting Brownian particles and find that the threshold value for the emergence of the flux depends on the coupling strength between interacting particles and the number of the particles. This implies that different coupling strengths or amounts of the particles correspond to different rectifications. Moreover, the magnitude of the flux is almost a constant with the varying bias in certain parameter regimes, revealing that there exits a collective motion in interacting particles.

Taken together, our work reveals the underlying mechanism for the rectification of the flux in the system consisting of two substrate potentials. Comparing our work with the rectification of Brownian motion discussed in earlier work [5,49], we come to two conclusions. One is that our results play an important role in the tuned control rectification of Brownian motion. The other is that we present the underlying mechanism of the rectification in a universal model, which is analyzed via the IE and dynamical relaxation of the diffusion. Therefore it provides not only a way of the rectification for the transports of various particles from the nanoscale to the mesoscale (e.g., ions, electrons, phonons, motile bacteria, nanoswimmers, Brownian particles, etc.), but also a design of various circuits. This circuit of Josephson junctions, which consists of different resistances and capacitances, was studied in earlier works [71,72]. They showed the realization for the occurrence of a voltage rectification.

ACKNOWLEDGMENTS

This work was supported by the Yunnan Fundamental Research Projects (Grants No. 2019FI002, No. 202101AS070018, and No. 202101AV070015), Yunnan Province Ten Thousand Talents Plan Young and Elite Talents Project, and Yunnan Province Computational Physics and Applied Science and Technology Innovation Team.

APPENDIX A: THE DYNAMICAL BEHAVIORS OF THE DETERMINISTIC MODEL

To further understand the dynamical relaxation corresponding to the rectification, we present the phase-space map and power spectrum density (PSD) corresponding to $F = -0.8, -0.3, -0.01, 0.1, 0.3$, and 0.8 for different initial conditions in Fig. 7. Moreover, we employ 10^6 data of time series to plot the phase-space map and 2^{14} data of time series to calculate PSD. For $F = -0.8$ and $v_0 = 0.0$, the particle jumps from the initial wells to the left wells for $q_0 = 0.0$ in Fig. 7(a) but remains in the initial wells for $q_0 = 0.3$ in Fig. 7(d). These behaviors suggest that the motion of the particle is sensitive to the initial conditions, and the corresponding ensemble average of the velocities is negative. That the motion is sensitive to the initial conditions suggests that there might exist chaos in the system [66]. On the other hand, for $F = 0.8$, the particle moves from the initial substrate well to the right wells for $q_0 = 0.0$ and $v_0 = 0.0$ in Fig. 7(g) but stays in the initial well for $q_0 = 1.0$ and $v_0 = -0.2$ in Fig. 7(j). These behaviors imply that the ensemble average of the velocities is positive. It should be noted that for the same time evolution, the distance of the particle for $F = 0.8$ in Fig. 7(a) is larger than that for $F = -0.8$ in Fig. 7(j), and therefore the rectification of the flux appears. Additionally, the PSDs corresponding to remaining in the initial well are equal to each other, and the PSD for $F = -0.8$ does not match that for $F = 0.8$, as shown in Fig. 7(m). We also note that for $F = -0.8$, the velocities in Fig. 7(a) have both negative and positive, suggesting the system is disordered and in the nonlinear response regime,

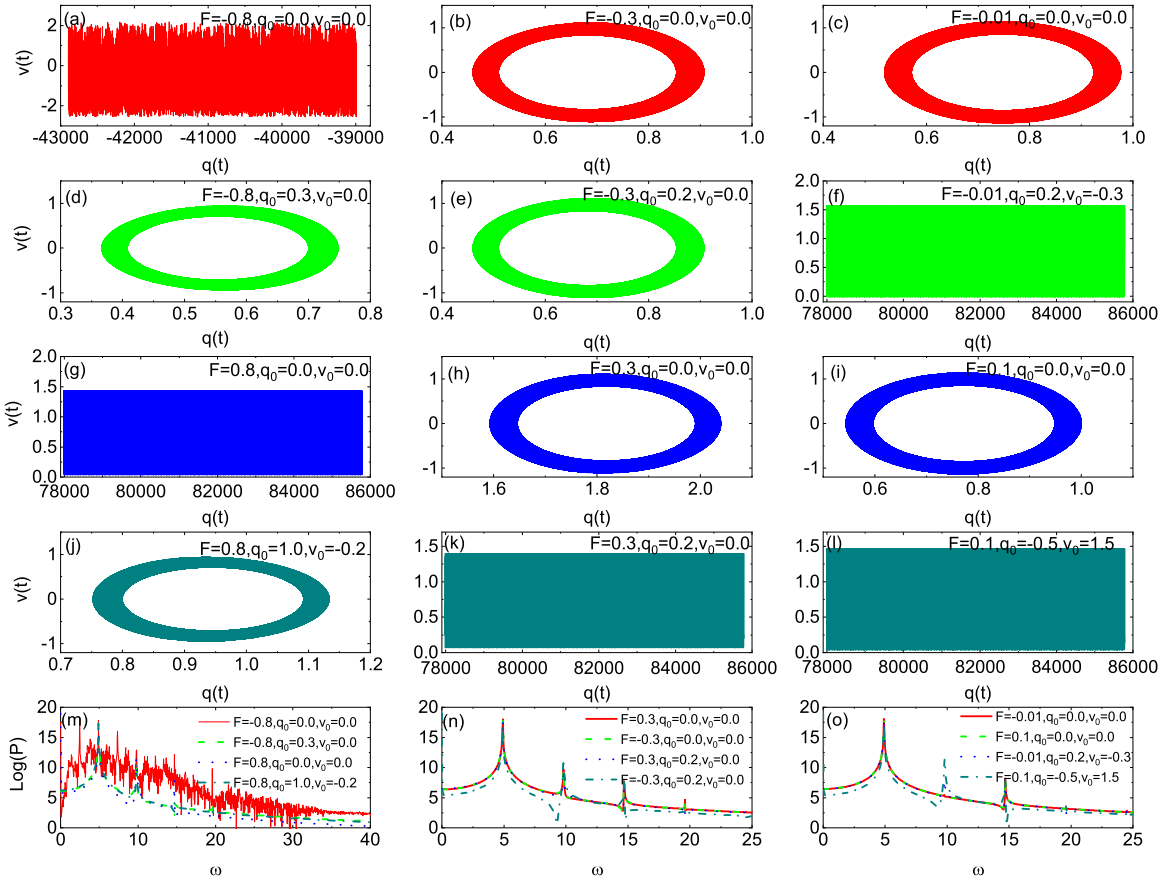

FIG. 7. The phase-space map and power spectra for $F = -0.8$, -0.3, -0.01, 0.1, 0.3 and 0.8. The other parameters are $\gamma_r = 0.7$ and $\lambda = 0.2$.

whereas for $F = 0.8$, the velocities in Fig. 7(j) are positive, implying that the system may be ordered and in a linear response regime. For $F = -0.3$, the phase-space map shows that the particle remains in the initial substrate well for different initial conditions in Figs. 7(b) and 7(e), implying that the ensemble average of the velocities is zero. Contrarily, for $F = 0.3$ and $v_0 = 0.0$, the time evolution shows that the particle moves from the initial well to the right wells for $q_0 = 0.2$ in Fig. 7(k) but remains in the initial well for $q_0 = 0.0$ in Fig. 7(h), suggesting that the ensemble average of the velocities is positive. As a result, the average velocity for $F = 0.3$ is larger than that for $F = -0.3$, implying the appearance of the rectification. Moreover, the PSDs corresponding to staying in the initial well are identical to each other, whereas they are not in agreement with those of the particle moving from the initial well to others, as shown in Fig. 7(n). For $F = -0.01$, the phase-space map shows that the particle stays in the initial well for $q_0 = 0.0$ and $v_0 = 0.0$ in Fig. 7(c) and moves from the initial well to right wells for $q_0 = 0.2$ and $v_0 = -0.3$ in Fig. 7(f), suggesting that the ensemble average is positive. Therefore the ratchet effects may arise. Moreover, at $F = 0.1$, some conditions lead to positive mobility, whereas the others give rise to zero mobility, as shown in Figs. 7(i) and 7(l). Furthermore, their PSDs are presented in Fig. 7(o), which shows that different driving forces have different PSDs except those corresponding to staying in the initial well. In brief, the phase-space map suggests that certain parameters and initial conditions lead to the rectification of the flux of the particle in the system.

APPENDIX B: THE DEPENDENCE OF THE DIFFUSION AND PROBABILITY DISTRIBUTION ON THERMAL NOISE

To better understand the dependence of the rectification on thermal noise in Fig. 3, we present the MSD and TDC in Fig. 8 and the probability distribution of the velocity $P(v)$ in Fig. 9.

Figure 3(e) shows that at low temperature (e.g., $T < 10^{-2}$), $D_+(t)$ is nontrivial, which corresponds to ballistic diffusion in Fig. 8(a), and the color changes from the light red to the deep red with time t in Fig. 8(e) for $T = 10^{-4}$, implying superdiffusion. On the other hand, the TDC $D_-(t)$ is nearly equal to zero, which is also proved for $T = 10^{-4}$ in Figs. 8(a) and 8(i). For J_- at low temperature, Fig. 8(a) shows that the MSD scales as $t^{0.7}$ or decreases with time t, and Fig. 8(i) shows that the color of $D_-(t)$ changes from the deep green to the light green with time t. These findings suggest that the diffusion of the particle is subdiffusive first and finally converges to zero. As the temperature increases (*e.g.*, $T = 10^{-2}$), $D_+(t)$ is smaller than $D_-(t)$ in Fig. 3(e). The reason is shown in Fig. 8(e), which shows that for $T = 10^{-2}$, the color of $D_+(t)$ changes from the red to the light red with time t, implying that the corresponding diffusion is subdiffusive first and then normal or converges to zero. However, $D_-(t)$ with $T = 10^{-2}$ shows a transition from the green into the deep green

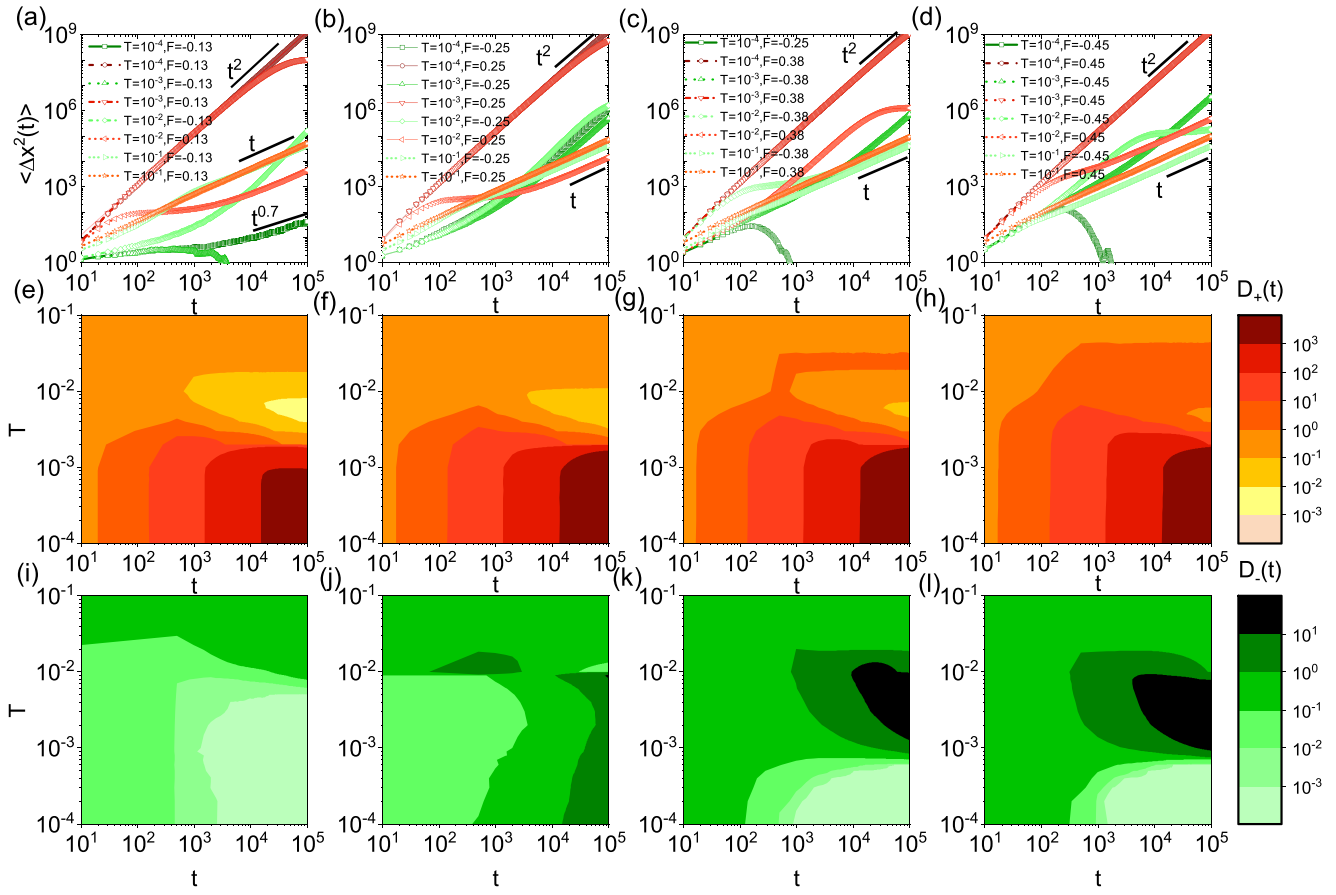

FIG. 8. MSD $\langle \Delta x^2(t) \rangle$ (the first row), TDC $D_+(t)$ (the second row), TDC $D_-(t)$ (the third row) vs time for different biases of Fig. 3. The other parameters are the same as in Fig. 3.

in Fig. 8(i), suggesting that the diffusion is superdiffusive. Upon further increasing the temperature (e.g., $T = 10^{-1}$), Fig. 3(e) shows that $D_+(t)$ is slightly larger than $D_-(t)$ again. This is also demonstrated in Figs. 8(a) and 8(e), which show that both MSDs in Fig. 8(a) scale as time t and both the colors of TDCs in Figs. 8(e) and 8(i) do not change with time t. Therefore both diffusions belong to normal diffusion, and $D_+(t)$ is larger than $D_-(t)$. Notice that at low temperature (e.g., T ranging from 10^{-4} to 10^{-3}), $D_-(t)$ is nearly equal to zero, and the flux J_- disappears as well. These results suggest that the particle does not overcome the left potential barrier and remains in the initial well. On the other hand, the flux J_+ and $D_+(t)$ are nontrivial, and the corresponding MSD shows that the diffusion is ballistic. S_+ also is larger than S_-, namely, the states of the velocities for $F > 0.0$ are more than those for $F < 0.0$. These findings imply that the particle overcomes the right potential barrier and jumps from the initial wells to the right wells. This is demonstrated in Fig. 9(a), which shows that $P(v)$ corresponding to $F = 0.13$ is wider than that corresponding to $F = -0.13$ for $T = 10^{-4}$. It is also shown that $P(v)$ has both negative and positive velocities and is symmetrical around $v = 0.0$ for $F = -0.13$. Thus this weakens the diffusion and mobility of the particle. However, $P(v)$ corresponding to $F = 0.13$ is asymmetrical, and thus it enhances the diffusion and mobility of the particle, which matches the results of Figs. 3(a) and 3(e).

As T increases (e.g., $T = 2 \times 10^{-3}$), both fluxes are almost equal to zero, $D_\pm(t)$ are very small, and S_+ is almost equal to S_-. The reason is presented in Fig. 9(e), which shows that $P(v)$ corresponding to $F = -0.13$ and 0.13 are almost symmetrical around $v = 0.0$. These distributions of negative and positive velocities are equal to each other, implying that they weaken the diffusion and mobility of the particle. Upon increasing T (e.g., $T = 10^{-2}$), $|J_-|$ is almost equal to J_+, and $D_+(t)$ and S_+ are smaller than $D_-(t)$ and S_-, respectively. These results are analyzed as follows. The corresponding $P(v)$ is plotted in Fig. 9(i), which shows that $P(v)$ for $F = -0.13$ is wider than that for $F = 0.13$. Moreover, both are almost symmetrical around $v = 0.0$, which suppresses the diffusion and mobility. At $T = 10^{-1}$, MSDs for $F = -0.13$ and 0.13 scale as time [Fig. 8(a)], and the corresponding colors of $D_+(t)$ and $D_-(t)$ do not change with time. The reason is given in Fig. 9(m), which shows that $P(v)$ for $F = -0.13$ is wider than that for $F = 0.13$. Both $P(v)$ are asymmetrical, which enhances the diffusion and mobility of the particle. In a word, these results reveal that the asymmetry of the $P(v)$ of the negative and positive velocities can promote diffusion and mobility in the disordered system.

We present the MSD and TDC versus time in Figs. 8(b) and 8(f) for $F = 0.25$. At low temperature (e.g., $T = 10^{-4}$), the diffusion corresponding to $F = 0.25$ is ballistic in Fig. 8(b), and the color of $D_+(t)$ changes from the light red to the deep red with time t in Fig. 8(f), implying that the corresponding diffusion is superdiffusive. Figure 8(b), however, shows that for $F = -0.25$, the MSD scales as time t^β with $1 < \beta \leqslant 2$. Thus the diffusion is superdiffusive, which is

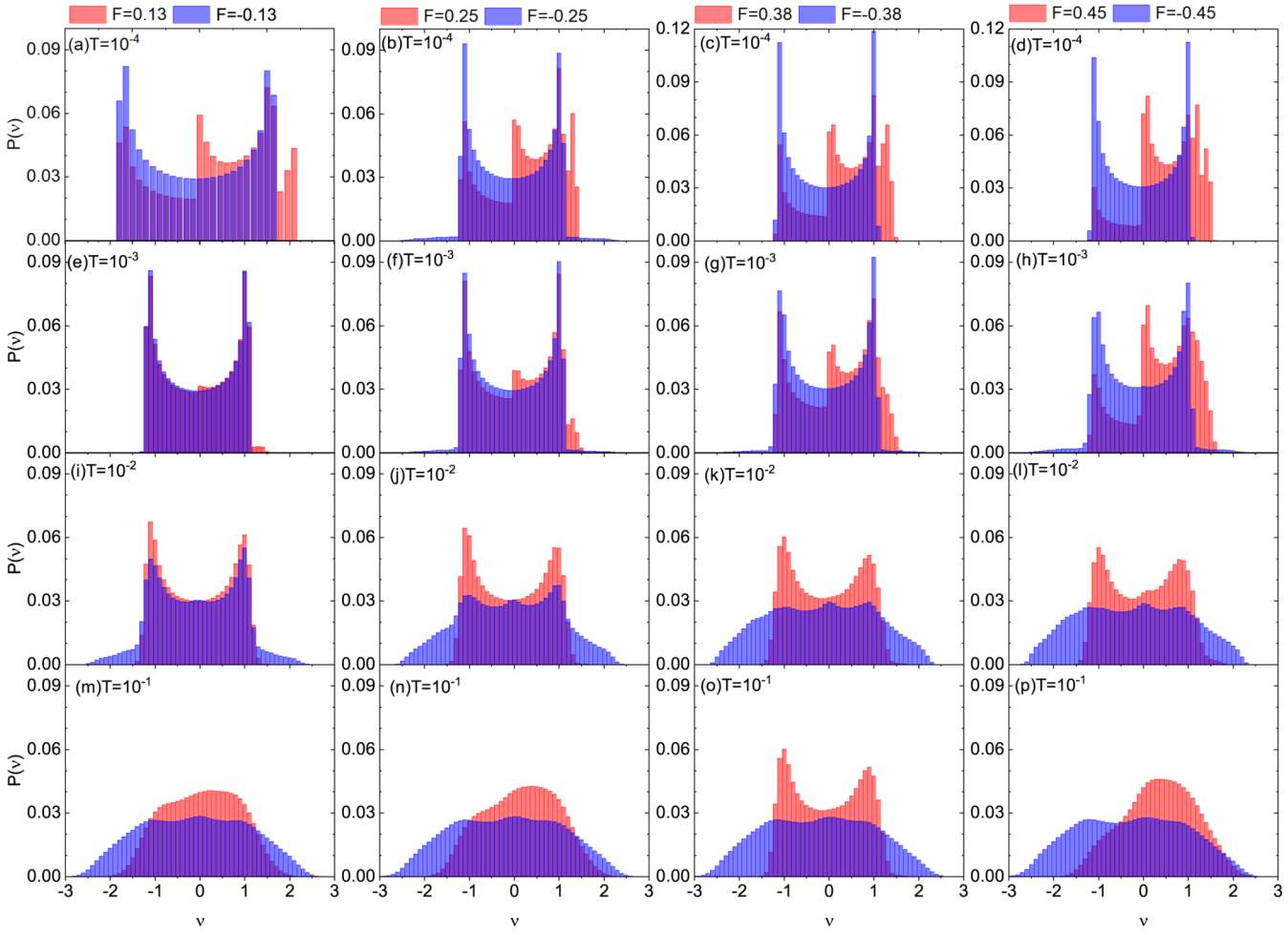

FIG. 9. The probability distribution of the velocity $P(v)$ corresponding to $T = 10^{-4}$ (the first row), 10^{-3} (the second row), 10^{-2} (the third row), and 10^{-1} (the fourth row) for different biases of Fig. 3. The other parameters are the same as in Fig. 3.

also supported in Fig. 8(j), showing that the color of $D_-(t)$ changes from the light green to the deep green. It suggests that the corresponding diffusion is superdiffusive. At $T = 10^{-2}$, the corresponding diffusion is normal for $F = 0.25$, whereas it is superdiffusive and then becomes subdiffusive for $F = -0.25$. At $T = 10^{-1}$, the colors of $D_+(t)$ and $D_-(t)$ do not change with time t, implying that the corresponding diffusions are normal for both $F = 0.25$ and -0.25. Furthermore, S_+ slightly decreases at $T = 10^{-3}$ and then increases with the increase of the temperature T whereas S_- roughly increase with increasing the temperature T in Fig. 3(j), implying that the system is more disordered with increasing T. These findings are analyzed in Figs. 9(b), 9(f), 9(j), and 9(n). Figure 9(b) shows that $P(v)$ corresponding to $F = 0.25$ is asymmetrical for $T = 10^{-4}$, suggesting that it enhances diffusion and mobility, which is in agreement with the results of Figs. 3(b) and 3(f). However, $P(v)$ corresponding to $F = -0.25$ is wider than that corresponding to $F = 0.25$, which suggests $S_- > S_+$. The distribution for $F = -0.25$ is almost symmetrical around $v = 0.0$, which weakens the diffusion and mobility and matches the results of Figs. 3(b) and 3(f) as well. For $T = 10^{-3}$, although $P(v)$ for $F = -0.25$ is wider than that for $F = 0.25$ which implies $S_- > S_+$, $P(v)$ for $f = 0.25$ is asymmetrical while $P(v)$ for $f = -0.25$ almost symmetrical around $v = 0.0$ in Fig. 9(f). Therefore the corresponding diffusion and mobility for $f = 0.25$ and -0.25 are enhanced and suppressed, respectively, which are identical to the results of Figs. 3(b) and 3(f). For $T = 10^{-2}$, both $P(v)$ are asymmetric in Fig. 9(j). It is also shown that $P(v)$ for $F = -0.25$ is wider than that for $F = 0.25$, thus the diffusion and flux for $F = -0.25$ are larger than those for $F = 0.25$ [Figs. 3(b) and 3(f)]. For $T = 10^{-1}$, both $P(v)$ are apparently asymmetrical around $v = 0.0$ in Fig. 9(n). It is shown that $P(v)$ for $F = -0.25$ is wider than that for $F = 0.25$, which means $S_- > S_+$, whereas the diffusion and flux for the former are smaller than those for the latter in Figs. 3(b) and 3(f).

For $F = 0.38$ and 0.45, the TDC in Figs. 8(c), 8(d), 8(g), 8(h), 8(k), and 8(l) and $P(v)$ in Figs. 9(c), 9(d), 9(g), 9(h), 9(k), 9(l), 9(o), and 9(p) match the corresponding fluxes in Figs. 3(c) and 3(d).

APPENDIX C: THE EFFECT OF THE BIAS ON THE RECTIFICATION

To address the issue of how the bias influences the rectification, we plotted the fluxes, TDCs, IEs, rectifying efficiency, and rectification coefficient versus the bias in Fig. 10. The

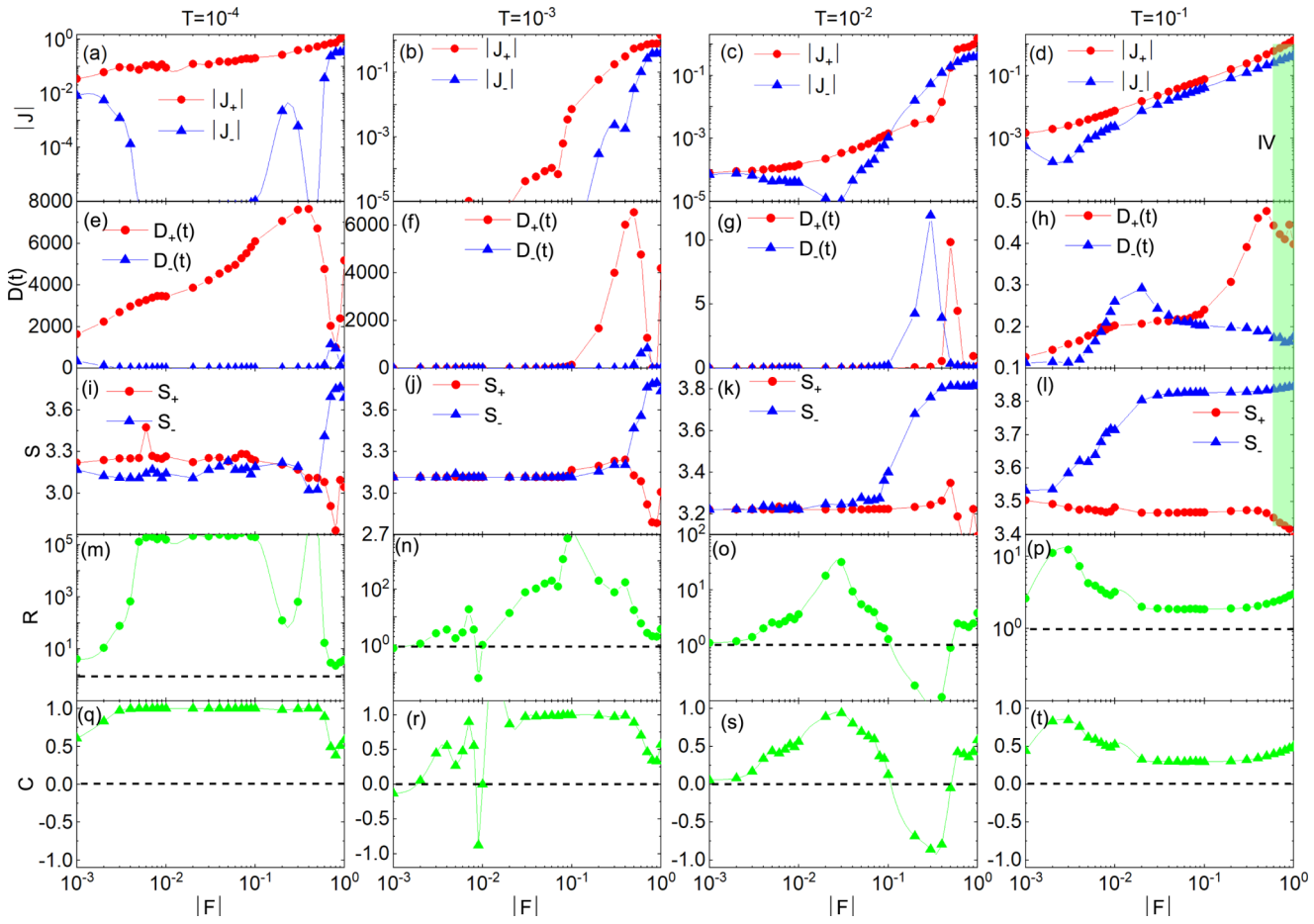

FIG. 10. The flux of the particle (the first row), TDC $D(t)$ with $t = 10^5$ (the second row), IE S (the third row), rectifying efficiency (the fourth row), and rectification coefficient (the fifth row) as functions of the bias for $T = 10^{-4}$ (the first column), 10^{-3} (the second column), 10^{-2} (the third column), and 10^{-1} (the fourth column). The other parameters are $\gamma_r = 0.7$ and $\lambda = 0.2$.

reason why these findings happen is analyzed via TDC in Fig. 11 and $P(v)$ in Fig. 12.

When $T = 10^{-4}$, Fig. 10(a) shows that J_+ corresponding to F is larger than J_- corresponding to $-F$, implying that the system has a perfect rectification. This can be supported by Figs. 10(e), 10(i), 10(m), and 10(q). Figure 10(e) shows that $D_+(t)$ with $t = 10^5$ is nontrivial, whereas $D_-(t)$ with $t = 10^5$ is trivial or nearly zero. Let us take a closer look at IE: Fig. 10(i) shows that for a nonlinear response regime (e.g., $F < 0.1$), S_+ is larger than S_-, which is in agreement with the findings of Fig. 10(a). However, in a nearly linear regime (e.g., $F > 0.5$), the S_+ is smaller than S_-. Moreover, the rectifying efficiency and rectification coefficient are presented in Figs. 10(m) and 10(q), respectively, which show that for $T = 10^{-4}$, the system has the prefect rectification for F ranging from 3×10^{-3} to 0.5. We now turn to the TDC. Figure 11(a) shows that for a small negative bias (i.e., $F = -0.01$ or -0.001), MSDs grow with t^2 at a short time and converge to a constant at the long-time limit, indicating superdiffusions at short time and then subdiffusion at the long-time limit or converging to zero finally, which are demonstrated in Fig. 11(i). Moreover, for a positive bias (e.g., $F = 0.01$, or 1.0), the corresponding MSD is proportional to t^2, revealing that the diffusion is ballistic. On the other hand, the corresponding MSD roughly converges to a constant at the long-time limit for a certain negative bias (i.e., $F = -0.1$), suggesting that the diffusion converges to zero. Moreover, the corresponding MSD shows that the diffusion is ballistic for $F = -1.0$. These results are also shown through TDC in Figs. 11(e) and 11(i). For a positive bias (i.e., $F = 0.01$ or 0.1), the color of TDC changes from the light red to the deep red with time t, meaning that the corresponding diffusion is superdiffusive. On the other hand, for a trivial negative bias, Fig. 11(i) shows that the color of $D_-(t)$ changes from the light green to the deep green first, and then from the deep green to the light green with time t, suggesting that the corresponding diffusion is superdiffusive first and then becomes subdiffusive. As the bias increases, certain biases (i.e., $F = -0.02$, -0.05, or -0.4) lead to the color of $D_-(t)$ changing from the green to the light green with time t, suggesting that the corresponding diffusion is subdiffusive, whereas the other biases (e.g., $F = -0.2$ or -0.8) give rise to the result that it changes from the green to the deep green with time t, revealing that the corresponding diffusion is superdiffusive.

Furthermore, we also present the corresponding $P(v)$ in Fig. 12. Figure 12(a) shows that $P(v)$ corresponding to $F = 0.001$ is trivially asymmetrical and that corresponding to $F = -0.001$ is almost symmetrical around $v = 0.0$, thus the former enhances the transport whereas the latter weakens it. Moreover, for larger positive biases, the distributions are

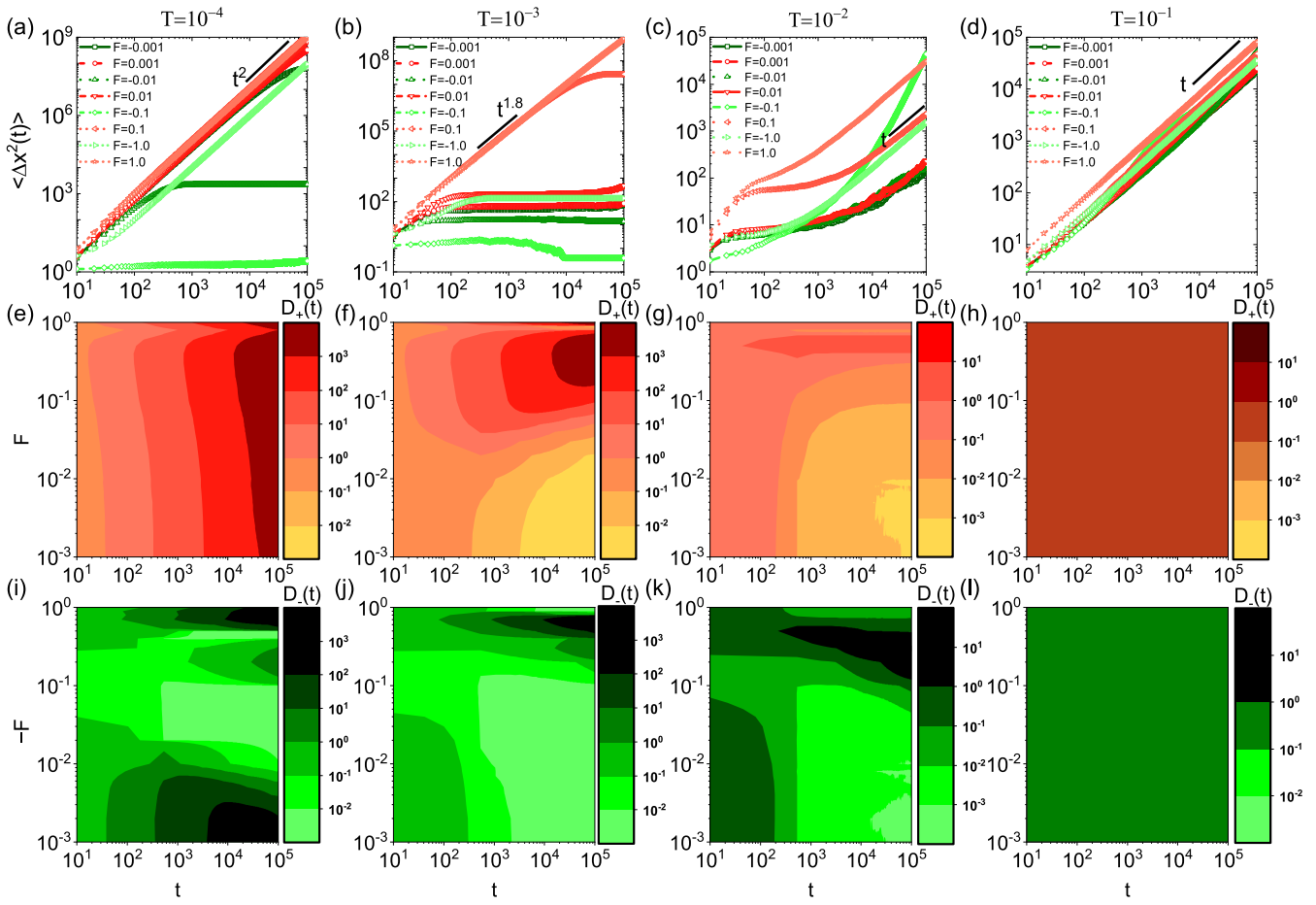

FIG. 11. The MSD (the first row), TDC $D_+(t)$ (the second row), and $D_-(t)$ (the third row) as functions of time for $T = 10^{-4}$ (the first column), 10^{-3} (the second column), 10^{-2} (the third column), and 10^{-1} (the fourth column). The other parameters are $\gamma_r = 0.7$ and $\lambda = 0.2$.

asymmetrical, as shown in Figs. 12(e) and 12(i) (red columns). This phenomenon can enhance the corresponding diffusions and fluxes. These findings suggest that for these biases, the system may be in disorder and in the nonlinear response regime. However, it should be noted that for $F = 1.0$, the velocities are almost positive in Fig. 12(m), implying that the system may be in order and in the linear response regime. Contrarily, $P(v)$ corresponding to $F = -0.01$ and -0.1 are perfectly symmetrical around $v = 0.0$, as shown in Figs. 12(e) and 12(i) (blue columns). This can weaken the corresponding diffusions and fluxes. Additionally, $P(v)$ is asymmetrical for $F = -1.0$ in Fig. 12(m). For these biases, the velocities are negative and positive, implying that the system may be in disorder and in the nonlinear response regime. These results are consistent with those of Fig. 10.

When $T = 10^{-3}$, Fig. 10(b) shows that both J_+ and J_- are smaller than 10^{-4} for $|F| < 3 \times 10^{-2}$, thus the results of rectification may be meaningless. For large biases (e.g., $|F| = 0.2$), however, the forward flux is larger than the reverse flux, implying that the rectification effect arises. The corresponding TDC $D_+(t)$ and $D_-(t)$ with $t = 10^5$ are trivial for a small driving F and the $D_+(t)$ is larger than the $D_-(t)$ for a large driving F in Fig. 10(f). In fact, for a small driving F, there exists no diffusion, which is also supported by Figs. 11(b), 11(f), and 11(j). Figure 11(b) shows that for large driving F (e.g., $F = 0.1$ or $F = 1.0$), $\langle \Delta x^2(t) \rangle$ is proportional to $t^{1.8}$ at short times and for $F = 0.1$, it converges to a constant at long times, implying that the particle may undergo superdiffusion first and then become subdiffusive or nondiffusive. For negative and small positive driving F, MSDs converge to a constant at long times, implying that the diffusion is subdiffusive first and then converges to zero. These results are also shown in Figs. 11(f) and 11(j). More reasons are presented in Figs. 12(b), 12(f), and 12(j), which show that for both cases of the negative and small positive biases, $P(v)$ are symmetrical around $v = 0.0$ and equal to each other. For large biases (e.g., $F = 1.0$ or -1.0), $P(v)$ are asymmetrical around $v = 0.0$, which can enhance the corresponding diffusion and flux. We also find that for a trivial bias, the rectifying efficiency and rectification coefficient fluctuate frequently, implying that these results are meaningless since the corresponding fluxes are very trivial, as shown in Figs. 10(n) and 10(r). But when $3 \times 10^{-2} < |F| < 7 \times 10^{-1}$, J_+ is larger than J_-, implying that nontrivial rectification occurs. This phenomenon is supported by the rectifying efficiency [Fig. 10(n)] and rectification coefficient [Fig. 10(r)]. Upon further increasing the bias (e.g., $|F| = 1.0$), J_+ almost equals J_-, and thus the rectification effect becomes trivial.

For $T = 10^{-2}$, Fig. 10(c) shows that J_+ is larger than J_- for $|F| < 0.2$, and therefore, there is a rectification. The unexpected phenomenon that J_- is larger than J_+ occurs for $0.2 < |F| < 0.5$. This result suggests that negative rectification ap-

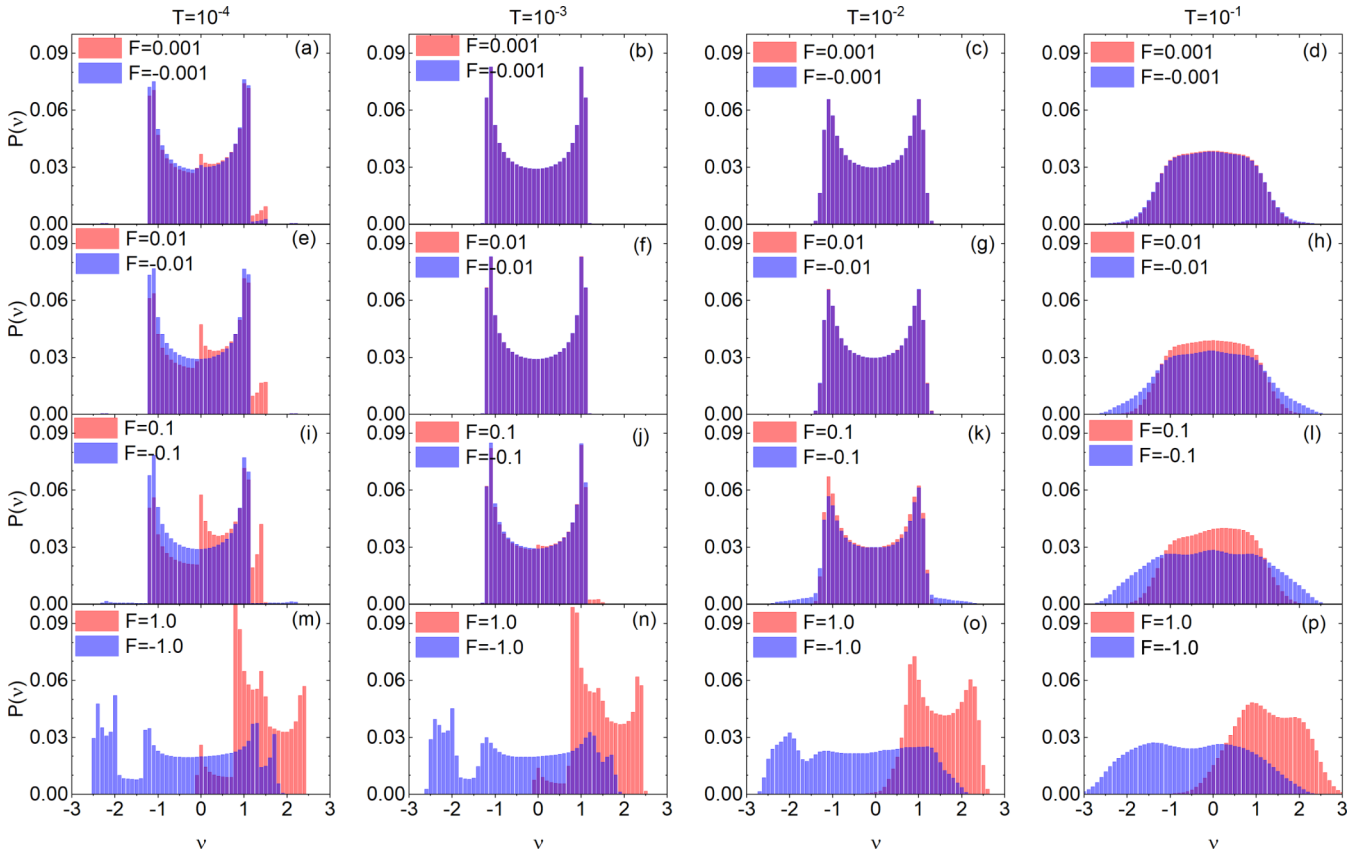

FIG. 12. The probability distributions $P(v)$ of the velocity for $T = 10^{-4}$ (first column), 10^{-3} (second column), 10^{-2} (third column), and 10^{-1} (fourth column). The other parameters are $\gamma_r = 0.7$ and $\lambda = 0.2$.

pears. The corresponding TDC and IE are given in Figs. 10(g) and 10(k). Figure 10(g) shows that for $|F| < 10^{-1}$, $D_+(t)$ is almost equal to $D_-(t)$ at $t = 10^5$. For $0.1 < |F| < 0.4$, on the other hand, $D_+(t)$ is smaller than $D_-(t)$. Upon further increasing the driving F, $D_+(t)$ is larger than $D_-(t)$. Let us look at IE: Fig. 10(k) shows that S_+ is almost equal to S_- for $|F| < 10^{-2}$, and S_+ is smaller than S_- for $|F| > 10^{-2}$. This implies that for the nonlinear response regime, the more disordered the system is, the larger are the flux and diffusion. For the linear response regime, however, the smaller IE S is, the larger the flux and TDC are. The explanation of these results is shown in Figs. 11 and 12. Figure 11(c) shows that MSDs scale as time t except $F = -0.1$, revealing that the corresponding diffusions are normal. More detailed explanations are shown in Figs. 11(g) and 11(k). For $F < 10^{-2}$, Fig. 11(g) shows that the color of $D_+(t)$ changes from the red to the light red with time t, implying that the corresponding diffusion is subdiffusive. For the bias ranging from $F = 10^{-2}$ to 1.0, there are three cases for diffusion. The first is that the color of $D_+(t)$ changes from the red to the light red at short time and does not change with time t at long times, revealing that the corresponding diffusions are subdiffusion at short times and normal at long times. The second is that the color of $D_+(t)$ does not change with time t, meaning that the diffusion is normal. The last is that the color of $D_+(t)$ changes from the red to the deep red at short times and does not change with time t, implying that the diffusion is superdiffusive at short times and normal at long time times. For negative bias, Fig. 11(k) shows that there are five kinds of diffusions. The first is that the color of $D_-(t)$ changes from the deep green to green with time t at short times and does not change with time t at long times, meaning that the diffusion is subdiffusive at short times and normal at long times, such as $F = -0.02$ or -1.0. The second is that the color of $D_-(t)$ changes from the deep green to the green at short times and then from the green to deep green at long times, implying that the diffusion is subdiffusive at short times and superdiffusion at long times, such as $F = -0.06$. The third is that the color of $D_-(t)$ changes from the deep green to the black first and then from the black to the green, revealing that the diffusion is superdiffusive first and then becomes subdiffusive, such as $F = -0.5$. The fourth case is that the color of $D_-(t)$ does not change with time, suggesting that the corresponding diffusion is normal, such as $F = -0.6$. The last is that the color of $D_-(t)$ changes from the deep green to green, then to the light green, implying that the diffusion is subdiffusive first, and converges to zero finally. More reasons are shown in Fig. 12. For the small bias, Figs. 12(c) and 12(g) show that $P(v)$ are symmetrical around $v = 0.0$ and equal to each other, implying that they weaken diffusion and flux. Figure 12(k) shows that $P(v)$ corresponding to $F = -0.1$ is wider than that corresponding to $F = 0.1$, and they both are almost symmetrical around $v = 0.0$, suggesting that the S_- corresponding to $F = -0.1$ is larger than S_+ corresponding to $F = 0.1$. This matches the results of Fig. 10(k). For these biases, there exist $P(v)$ with both negative and positive velocities, and thus the system may be disordered for them. However, Fig. 12(o)

shows that $P(v)$ corresponding to $F = 1.0$ are almost positive, whereas there exists the distribution with both negative and positive velocities for $F = -1.0$, meaning that the system is ordered for $F = 1.0$ but disordered for $F = -1.0$. It is also shown that $P(v)$ corresponding to $F = -1.0$ is wider than that corresponding to $F = 1.0$. All of them are in agreement with the results of Fig. 10.

When $T = 0.1$, Fig. 10(d) shows that J_+ is slightly larger than J_- with varying the bias, suggesting that the rectification of the flux is trivial. The rectifying efficiency and rectification coefficient have supported these findings, as shown in Figs. 10(p) and 10(t), respectively. Moreover, Fig. 10(h) shows that the $D_+(t)$ is larger than $D_-(t)$ for most of the biases, and $D_+(t)$ is smaller than $D_-(t)$ for a few of the bias. Additionally, Fig. 10(l) shows that S_+ is smaller than S_-. The analysis of these findings is given in Figs. 11(d), 11(h), and 11(l). Figure 11(d) shows that all MSDs scale as time. Figures 11(h) and 11(l) show that the colors of $D_+(t)$ and $D_-(t)$ do not change with time. Both suggest that the diffusions are normal. The explanation of these findings is given in Figs. 12(d), 12(h), 12(l), and 12(p). Figure 12(d) shows that both $P(v)$ are symmetrical around $v = 0.0$ and equal to each other for $|F| = 0.001$. Moreover, Figs. 12(h) and 12(l) show that $P(v)$ corresponding to $F = 0.01$ and 0.1 are narrower than those corresponding to $F = -0.01$ and -0.1, respectively. Moreover, Fig. 12(h) shows that both $P(v)$ are basically symmetrical whereas Fig. 12(l) displays that both $P(v)$ are trivially asymmetrical. Notice that the system driven by these biases is disordered for $P(v)$ with both negative and positive velocities. Furthermore, as shown in Fig. 12(p), $P(v)$ corresponding to $F = 1.0$ is nontrivially asymmetric and that corresponding to $F = -1.0$ is trivial asymmetric at $v = 0.0$, implying the flux and diffusion corresponding to $F = 1.0$ are larger than those corresponding to $F = -1.0$.

In brief, the rectification is sensitive to the bias, therefore, it can tune the rectification. Additionally, comparing J_+ and J_- for different temperatures T, Figs. 10(a)–(d) show that the lower the temperature is, the wider the parameter range of perfect rectification is. It is also clear as shown from the rectification coefficient in Figs. 10(q)–10(t). Namely, the temperature can suppress the rectification in Brownian motion.

[1] F. Nori, Reversible diodes for moving quanta, Nat. Phys. **2**, 227 (2006).

[2] J. Stenhammar, R. Wittkowski, D. Marenduzzo, and M. E. Cates, Light-induced self-assembly of active rectification devices, Sci. Adv. **2**, e1501850 (2016).

[3] D. Segal and A. Nitzan, Heat rectification in molecular junctions, J. Chem. Phys. **122**, 194704 (2005).

[4] H. Atesci, V. Kaliginedi, J. A. Celis Gil, H. Ozawa, J. M. Thijssen, P. Broekmann, M. A. Haga, and S. J. van der Molen, Humidity-controlled rectification switching in ruthenium-complex molecular junctions, Nat. Nanotechnol. **13**, 117 (2018).

[5] Y. F. He, B. Q. Ai, C. X. Dai, C. Song, R. Q. Wang, W. T. Sun, F. C. Liu, and Y. Feng, Experimental Demonstration of a Dusty Plasma Ratchet Rectification and Its Reversal, Phys. Rev. Lett. **124**, 075001 (2020).

[6] B. Li, L. Wang, and G. Casati, Thermal Diode: Rectification of Heat Flux, Phys. Rev. Lett. **93**, 184301 (2004).

[7] N. Li, J. Ren, L. Wang, G. Zhang, P. Hänggi, and B. Li, Colloquium: Phononics: Manipulating heat flow with electronic analogs and beyond, Rev. Mod. Phys. **84**, 1045 (2012).

[8] B. C. Lee, G. Khelashvili, M. Falzone, A. K. Menon, H. Weinstein, and A. Accardi., Gating mechanism of the extracellular entry to the lipid pathway in a TMEM16 scramblase, Nat. Commun. **9**, 3251 (2018).

[9] Z. Zhang, X. Y. Kong, K. Xiao, G. Xie, Q. Liu, Y. Tian, H. Zhang, J. Ma, L. Wen, and L. Jiang, A bioinspired multifunctional heterogeneous membrane with ultrahigh ionic rectification and highly efficient selective ionic gating, Adv. Mater. **28**, 144 (2016).

[10] V. Mujica, M. A. Ratner, and A. Nitzan, Molecular rectification: Why is it so rare? Chem. Phys. **281**, 147 (2002).

[11] D. R. Ward, F. Hüser, F. Pauly, J. C. Cuevas, and D. Natelson, Optical rectification and field enhancement in a plasmonic nanogap, Nat. Nanotechnol. **5**, 732 (2010).

[12] J. Dai, A. Roulet, H. Nguyen Le, and V. Scarani, Rectification of light in the quantum regime, Phys. Rev. A **92**, 063848 (2015).

[13] V. Balachandran, G. Benenti, E. Pereira, G. Casati, and D. Poletti, Perfect Diode in Quantum Spin Chains, Phys. Rev. Lett. **120**, 200603 (2018).

[14] M. J. Martínez-Pérez, A. Fornieri, and F. Giazotto, Rectification of electronic heat current by a hybrid thermal diode, Nat. Nanotechnol. **10**, 303 (2015).

[15] P. A. Camati, J. P. S. Peterson, T. B. Batalhão K. Micadei, A. M. Souza, R. S. Sarthour, I. S. Oliveira, and R. M. Serra, Experimental Rectification of Entropy Production by Maxwell's Demon in a Quantum System, Phys. Rev. Lett. **117**, 240502 (2016).

[16] M. F. Carusela and J. M. Rubí, Entropic rectification and current inversion in a pulsating channel, J. Chem. Phys. **146**, 184901 (2017).

[17] M. F. Carusela and J. Miguel Rubí, Entropy production and rectification efficiency in colloid transport along a pulsating channel, J. Phys.: Condens. Matter **30**, 244001 (2018).

[18] Y. F. Chen, S. Xiao, H. Y. Chen, Y. J. Sheng, and H. K. Tsao, Enhancing rectification of a nano-swimmer system by multilayered asymmetric barriers, Nanoscale **7**, 16451 (2015).

[19] Y. F. Chen, H. Y. Chen, Y. J. Sheng, and H. K. Tsao, Directed drift and fluid pumping of nanoswimmers by periodic rectification-diffusion, J. Chem. Phys. **146**, 014902 (2017).

[20] P. Hänggi and F. Marchesoni, Artificial Brownian motors: Controlling transport on the nanoscale, Rev. Mod. Phys. **81**, 387 (2009).

[21] H. Cho *et al.*, The calcium-activated chloride channel anoctamin 1 acts as a heat sensor in nociceptive neurons, Nat. Neurosci. **15**, 1015 (2012) .

[22] G. Xie, P. Li, Z. Zhang, K. Xiao, X.-y. Kong, L. Wen, and L. Jiang, Skin-inspired low-grade heat energy harvesting using

directed ionic flow through conical nanochannels, Adv. Energy Mater. **8**, 1800459 (2018).

[23] A. M. Peier, A. J. Reeve, D. A. Andersson *et al.*, A heat-sensitive TRP channel expressed in keratinocytes, Science **296**, 2046 (2002).

[24] F. Ando, Y. Miyasaka, T. Li, J. Ishizuka, T. Arakawa, Y. Shiota, T. Moriyama, Y. Yanase, and T. Ono, Observation of superconducting diode effect, Nature (London) **584**, 373 (2020).

[25] R. Fleury, D. L. Sounas, C. F. Sieck, M. R. Haberman, and A. Alù, Sound isolation and giant linear nonreciprocity in a compact acoustic circulator, Science **343**, 516 (2014).

[26] C. Coulais, D. Sounas, and A. Alù, Static non-reciprocity in mechanical metamaterials, Nature (London) **542**, 461 (2017).

[27] H. Xu, L. Jiang, A. A. Clerk, and J. G. E. Harris, Nonreciprocal control and cooling of phonon modes in an optomechanical system, Nature (London) **568**, 65 (2019).

[28] Y. Wang, B. Yousefzadeh, H. Chen, H. Nassar, G. Huang, and C. Daraio, Observation of Nonreciprocal Wave Propagation in a Dynamic Phononic Lattice, Phys. Rev. Lett. **121**, 194301 (2018).

[29] A. Einstein, Über die von der molekularkinetischen Theorie der Wärme geforderte Bewegung von in ruhenden Flüssigkeiten suspendierten Teilchen, Ann. Phys. **322**, 549 (1905).

[30] Y. Han, A. M. Alsayed, M. Nobili, J. Zhang, T. C. Lubensky, and A. G. Yodh, Brownian motion of an ellipsoid, Science **314**, 626 (2006).

[31] T. Li, S. Kheifets, D. Medellin, and M. G. Raizen, Measurement of the instantaneous velocity of a Brownian particle, Science **328**, 1673 (2010).

[32] S. Kheifets, A. Simha, K. Melin, T. Li, and M. G. Raizen, Observation of Brownian motion in liquids at short times: Instantaneous velocity and memory loss, Science **343**, 1493 (2014).

[33] T. Turiv, I. Lazo, A. Brodin, B. I. Lev, V. Reiffenrath, V. G. Nazarenko, and O. D. Lavrentovich, Effect of collective molecular reorientations on Brownian motion of colloids in nematic liquid crystal, Science **342**, 1351 (2013).

[34] H. Safdari, A. G. Cherstvy, A. V. Chechkin, A. Bodrova, and R. Metzler, Aging underdamped scaled Brownian motion: Ensemble- and time-averaged particle displacements, nonergodicity, and the failure of the overdamping approximation, Phys. Rev. E **95**, 012120 (2017).

[35] V. O. Kharchenko and I. Goychuk, Subdiffusive rocking ratchets in viscoelastic media: Transport optimization and thermodynamic efficiency in overdamped regime, Phys. Rev. E **87**, 052119 (2013).

[36] A. Xu, C. Lin, G. Zhang, and Y. Li, Multiple-relaxation-time lattice Boltzmann kinetic model for combustion, Phys. Rev. E **91**, 043306 (2015).

[37] F. Chen, A. Xu, Y. Zhang, and Q. Zeng, Morphological and non-equilibrium analysis of coupled Rayleigh-Taylor-Kelvin-Helmholtz instability, Phys. Fluids **32**, 104111 (2020).

[38] C. P. Koçer, K. J. Griffith, C. P. Grey, and A. J. Morris, Lithium diffusion in niobium tungsten oxide shear structures, Chem. Mater. **32**, 3980 (2020).

[39] K. J. Griffith, K. M. Wiaderek, G. Cibin, L. E. Marbella, and C. P. Grey, Niobium tungsten oxides for high-rate lithium-ion energy storage, Nature (London) **559**, 556 (2018).

[40] V. Lacivita, N. Artrith, and G. Ceder, Structural and compositional factors that control the li-ion conductivity in LiPON electrolytes, Chem. Mater. **30**, 7077 (2018).

[41] S. Bo and R. Eichhorn, Driven Anisotropic Diffusion at Boundaries: Noise Rectification and Particle Sorting, Phys. Rev. Lett. **119**, 060603 (2017).

[42] A. Orłowski, Information entropy and squeezing of quantum fluctuations, Phys. Rev. A **56**, 2545 (1997).

[43] E. Romera and F. de los Santos, Identifying Wave-Packet Fractional Revivals by Means of Information Entropy, Phys. Rev. Lett. **99**, 263601 (2007).

[44] J. Gieseler, R. Quidant, C. Dellago, and L. Novotny, Dynamic relaxation of a levitated nanoparticle from a non-equilibrium steady state, Nat. Nanotechnol. **9**, 358 (2014).

[45] T. Vicsek, A. Czirók, E. Ben-Jacob, I. Cohen, and O. Shochet, Novel Type of Phase Transition in a System of Self-Driven Particles, Phys. Rev. Lett. **75**, 1226 (1995).

[46] G. Grégoire and H. Chaté, Onset of Collective and Cohesive Motion, Phys. Rev. Lett. **92**, 025702 (2004).

[47] H. Chaté, F. Ginelli, G. Grégoire, and F. Raynaud, Collective motion of self-propelled particles interacting without cohesion, Phys. Rev. E **77**, 046113 (2008).

[48] R. Salgado-García, Noise-induced rectification in out-of-equilibrium structures, Phys. Rev. E **99**, 012128 (2019).

[49] B. Q. Ai, Y. F. He, and W. R. Zhong. Particle diode: Rectification of interacting Brownian ratchets, Phys. Rev. E **83**, 051106 (2011).

[50] F. Marchesoni and S. Savel'ev, Rectification currents in two-dimensional artificial channels, Phys. Rev. E **80**, 011120 (2009).

[51] B. Spagnolo, D. Valenti, C. Guarcello, A. Carollo, D. P. Adorno, S. Spezia, N. Pizzolato, and B. Di Paola, Noise-induced effects in nonlinear relaxation of condensed matter systems, Chaos Solitons Fractals **81**, 412 (2015).

[52] D. P. Adorno, N. Pizzolato, and B. Spagnolo, Noise-induced resonance-like phenomena in InP crystals embedded in fluctuating electric fields, J. Stat. Mech. Theory Exp. (2016) 054021.

[53] J. Zheng, X. Yan, L. Yu *et al.*, Family-dependent rectification characteristics in ultra-short graphene nanoribbon *p-n* junctions, J. Phys. Chem. C **115**, 8547 (2011).

[54] B. Vilozny, A. L. Wollenberg, P. Actis *et al.*, Carbohydrate-actuated nanofluidic diode: Switchable current rectification in a nanopipette, Nanoscale **5**, 9214 (2013).

[55] S. Umehara, N. Pourmand, C. D. Webb *et al.*, Current rectification with poly-L-lysine-coated quartz nanopipettes, Nano Lett. **6**, 2486 (2006).

[56] L. Yu, X. Yan, H. Li *et al.*, Negative rectification and negative differential resistance in nanoscale single-walled carbon nanotube *p-n* junctions, Theor. Chem. Acc. **130**, 353 (2011).

[57] R. Shrestha, Y. Luan, X. Luo *et al.*, Dual-mode solid-state thermal rectification, Nat. Commun. **11**, 4346 (2020).

[58] B. C. Bag, S. K. Banik, and D. S. Ray, Noise properties of stochastic processes and entropy production, Phys. Rev. E **64**, 026110 (2001).

[59] C. Grossert, M. Leder, S. Denisov, P. Hänggi, and M. Weitz, Experimental control of transport resonances in a coherent quantum rocking ratchet, Nat. Commun. **7**, 10440 (2016).

[60] D. A. Czaplewski, C. Chen, D. Lopez *et al.*, Bifurcation Generated Mechanical Frequency Comb, Phys. Rev. Lett. **121**, 244302 (2018).

[61] F. Kindermann, A. Dechant, M. Hohmann, T. Lausch, D. Mayer, F. Schmidt, E. Lutz, and A. Widera, Nonergodic diffusion of single atoms in a periodic potential, Nat. Phys. **13**, 137 (2017).

[62] R. Bartussek, P. Hänggi, and J. G. Kissner, Periodically rocked thermal ratchets, Europhys. Lett. **28**, 459 (1994).

[63] J. Spiechowicz, J. Łuczka, and P. Hänggi, Transient anomalous diffusion in periodic systems: Ergodicity, symmetry breaking and velocity relaxation, Sci. Rep. **6**, 30948 (2016).

[64] Y. Luo and C. Zeng, Negative friction and mobilities induced by friction fluctuation, Chaos **30**, 053115 (2020).

[65] R. L. Honeycutt, Stochastic Runge-Kutta algorithms. I. White noise, Phys. Rev. A **45**, 600 (1992).

[66] Y. Luo, C. Zeng, and B.-Q. Ai, Strong-chaos-caused negative mobility in a periodic substrate potential, Phys. Rev. E **102**, 042114 (2020).

[67] P. H. Guimarães, G. T. Landi, and M. J. de Oliveira, Thermal rectification in anharmonic chains under an energy-conserving noise, Phys. Rev. E **92**, 062120 (2015).

[68] A. Sarracino, F. Cecconi, A. Puglisi, and A. Vulpiani, Nonlinear Response of Inertial Tracers in Steady Laminar Flows: Differential and Absolute Negative Mobility, Phys. Rev. Lett. **117**, 174501 (2016).

[69] A. Hamma, W. Zhang, S. Haas, and D. A. Lidar, Entanglement, fidelity, and topological entropy in a quantum phase transition to topological order, Phys. Rev. B **77**, 155111 (2008).

[70] C. C. de Souza Silva, J. Van de Vondel, M. Morelle, and V. V. Moshchalkov, Controlled multiple reversals of a ratchet effect, Nature (London) **440**, 651 (2006).

[71] I. Zapata, R. Bartussek, F. Sols, and P. Hänggi, Voltage Rectification by a SQUID Ratchet, Phys. Rev. Lett. **77**, 2292 (1996).

[72] I. Zapata, J. Łuczka, F. Sols, and P. Hänggi, Tunneling Center as a Source of Voltage Rectification in Josephson Junctions, Phys. Rev. Lett. **80**, 829 (1998).